POLITECNICO DI MILANO

School of Industrial and Information Engineering

Department of Electronics, Information and Bioengineering

Master of Science in Biomedical Engineering

UNDERSTANDING THE MECHANISM OF DRUG PERFUSION THROUGH BRAIN TISSUE: HYDRAULIC PERMEABILITY STUDY

Supervisor: Prof. Elena DE MOMI

Co-supervisor: MSc Marco VIDOTTO

Dr Asad JAMAL

Prof. Daniele DINI

Author:

Maria Teresa MONGELLI, 899453

Academic Year 2018-2019

Dopo tanta

nebbia

a una

a una

si svelano

le stelle

G. Ungaretti

Ringraziamenti

Prima di entrare nel vivo della trattazione vorrei ringraziare chi mi ha sostenuto e aiutato nello sviluppare e redigere questa tesi.

Un doveroso ringraziamento va alla mia relatrice, la professoressa Elena De Momi, che mi ha dato l'opportunità di lavorare presso l'Imperial College London e al mio correlatore, Marco Vidotto, per il suo costante aiuto, anche a distanza, e per aver sopportato le mie ansie e le mie paure, con immensa pazienza.

Ringrazio di cuore il professore Daniele Dini, capo del Tribology Group presso l'Imperial College London. Nonostante i suoi numerosissimi e imprescindibili impegni, è sempre stato presente, sostenendomi e credendo fortemente in questa tesi.

From the depths of my heart I would like to thank my supervisor, Dr Asad Jamal, because he has guaranteed me professional growth thanks to his infinite advice, and personal growth, because his words have taught me to face my fears and to believe in myself.

Ringrazio infinitamente anche tutti i dottorandi che ho incontrato durante questa esperienza, oggi miei grandi amici. Ognuno, a suo modo mi ha introdotta nel mondo della ricerca, raccontandomi le proprie esperienze e integrandomi nel gruppo sin dal primo giorno. Non mi hanno mai fatta sentire sola in quel di Londra, e sono infatti divenuti lì, il mio punto di riferimento: A., C., Z., A., E., J., A., G., B.

Inoltre, sento la necessità di ringraziare chi, forse anche senza saperlo, ha contribuito nel raggiungimento di questo obiettivo.
I primi sono, senza dubbio ed alcuna esitazione, mia mamma e mio papà. A loro devo tutto. È grazie a voi e ai vostri Sacrifici se oggi sono qui, mi avete permesso di vivere nella città dei miei sogni senza farmi mancare mai nulla.

Grazie a mia sorella, la metà del mio cuore, che ha sofferto silenziosamente per la nostra distanza, alla sua testardaggine e al suo immenso coraggio che le invidieró per sempre.

Grazie a nonna Chiara e nonno Pasquale, perché i vostri sguardi e le vostre parole mi hanno insegnato l'amore, e il vostro supporto economico mi ha permesso di vivere tante esperienze.

Grazie a nonna Teresa e nonno Franco, ai mille ricordi che puntualmente mi riaffiorate, al pranzo che non mi fate mai mancare ogni volta che ritorno, a quella chiamata inevitabile ogni volta che vado via.

Grazie ai miei zii che mi hanno vista crescere e hanno creduto in me, e ai miei cugini, che ho visto crescere e che, nonostante io sia la più grande tra loro, non smettono di insegnarmi a sorridere sempre.

Grazie a te, M., alla tua infinita pazienza, all'amore percepibile nei tuoi "piccoli" gesti, nei tuoi occhi. A tutto quello che mi hai insegnato, perché mi ascolti, mi rimproveri e mi abbracci. Perché mi hai presentato una persona speciale, che mi riempie di gioia continuamente e mi ha insegnato cosa vuol dire amare la vita.

Grazie a te, F., sei stata la mia famiglia qui a Milano e lo sarai per sempre. Mi hai insegnato ad amare i cani, come fossero sorelle, mi hai insegnato quante vale una parola in un momento di difficoltà, mi hai insegnato a non avere paura.

Grazie a te, V., al tuo accento, al tuo sorriso, alla tua ansia perenne, perché è grazie a te che in tanti momenti sono riuscita a pensare a me stessa e a non colpevolizzarmi. E perché il Molise esiste ed è ricchissimo.

Grazie a te, E., perchè abbiamo passato anni mano nella mano, così a testa alta, mai l'una senza l'altra. Oggi siamo di nuovo qui a guardarci negli occhi, a ricordarci che forse niente è cambiato dentro di noi.

Grazie a te, S., perché la tua bellezza mi ha colpito dal primo giorno e sei la di-

mostrazione più grande che l'apparenza inganna. Sei dolce, magnanima, imprevedibile, coraggiosa, sincera.

Grazie a te, F., uno dei miei esempi più grandi, la milanese per eccellenza, una delle donne più intelligenti che abbia incontrato nel mio percorso, la prima laurea a cui ho assistito e la prima lode che ho sentito.

Grazie a te, I., perché ci siamo riscoperte, ritrovate e perché in fondo ci siamo mancate da morire, ma siamo sempre state indispensabili l'una per l'altra.

Grazie a te, V., il mio migliore amico, alle nostre serate, alle nostre risate, ai nostri segreti, al nostro essere sempre i soliti idioti, come se non ci fossimo mai allontanati.

Grazie a te, F., perché la tua poca dolcezza (solo apparente) è stata una sfida bellissima in questi ultimi due anni, i tuoi (troppi pochi) abbracci sono stati sempre il mio obiettivo giornaliero e le tua lunghissime chiamate mi hanno fatto capire che la distanza non esiste.

Grazie a te, G., al primo sguardo che ho incrociato qui al Politecnico. All'amore per il nostro sud che da subito ti è mancato, alle nostre promesse e alla tua vita incasinata.

Grazie a voi, F., M., M., al nostro gruppetto del primo anno, alle nostre cenette, alle nostre troppe poche uscite.

Grazie a voi, A. e M., che avete alleggerito questi anni con la vostra simpatia e la vostra amicizia vera, senza ndi voi nnon sarebbe stata lo stesso Poli.

Grazie a te, M., sempre distanti, asse Milano-Torino, ma sempre così vicine a un millimetro dal cuore.

Grazie a voi, D. e S., perché siete state una presenza importante in questi anni, con le nostre "pazze" serate e le nostre "strane" abbuffate.

Grazie a voi, V. e D., che dal liceo siete rimasti accanto a me e siete riusciti a non farmi sentire mai sola ogni volta che sono tornata a casa.

Grazie a Londra, la città dalle mille risorse, un crogiolo di culture, sempre troppo all'avanguardia, piena di segreti e di opportunità.

Grazie a Milano, la città che mi ha accolta con il suo Sole e perchè la sua immensità non mi ha mai fatto sentire sola. Mi ha fatto crescere e mi ha insegnato a vivere da sola, mi ha insegnato ad amare il nord, ma ancor di più mi ha insegnato a sognare il

sud.

Grazie alla mia Puglia, perché ti ho rivalutata e riscoperta, segno, forse, che per quanto lontana, un pezzo di te me lo porto sempre nel cuore.

Summary

Introduction

Glioblastoma multiforme (GBM) is one of the most frequent and malignant human brain tumours, remaining incurable in most cases, leaving patients a median overall survival rate ranging from 12 to 18 months [Mehta et al., 2015]. Conventional treatment involves, as a first approach, surgery, with which it is very challenging to remove all the tumour, and then radiation and/or chemotherapy that, overall, damage the tissue promoting systemic toxicity [Mehta et al., 2015]. In particular for chemotherapy, a major obstacle is represented by the blood-brain barrier (BBB) that significantly hinders the drug distribution thus preventing the drug from reaching the tumour.

From 1994, a new technique has been introduced in order to bypass the BBB, namely convection-enhanced delivery (CED), with promising results. With this method, intratumoural chemotherapies are administered by direct injection under positive pressure directly into the parenchyma. As the name suggests, convection is used to supplement diffusion and to introduce large and small molecules [Bobo et al., 1994]. However, the efficiency of this innovative technique is related to the ability to ensure the sufficient concentration of the drug in the targeted region [Mehta et al., 2015]. Its distribution depends on the region where it is infused, in fact homogeneous structure or structure containing fibres show different bulk flow pathways [Groothuis, 2000]. Different factors contribute to the good success of this treatment and, actually, rigorous computational models represent an important support. However, realistic values are necessary to im-

plement an accurate and reliable numerical model that includes the orientation of the white matter (WM) fibres tracts and the correct permeability and diffusion tensors [Støverud et al., 2012]. The determination of reliable hydraulic permeability values is still a subject of current research but it is a topic of deep interest in biological materials because of its important role in a range of drug delivery-based therapies. The strong dependence of permeability on the geometry and topology of the pore structure [Kapellos and Alexiou, 2013] and the lack of detailed knowledge of this parameter in the case of brain tissue makes the study more challenging. Although theoretical models have been developed for hydraulic permeability, the experimental evidence to complement these models is either lacking or still under discussion.

Aim of the work

In the present study, the authors measure the permeability of WM tract of fresh ovine brain tissue considering the localised heterogeneities using an infusion based experimental set-up, the *iPerfusion* [Sherwood et al., 2016]. The flow across different parts of the WM in response to applied pressures for a sample of specific dimensions was measured and the permeability from directly measured parameters was calculated. Furthermore, the effect of anisotropy of the tissue on permeability was directly investigated, by considering the directionality of tissue on the obtained values.

Additionally, it has been also probed if the hydraulic permeability of WM changes with post-mortem time.

State of the art

In the literature, a huge number of studies faces the problem of quantify the hydraulic permeability of porous media and specifically several soft tissue testing devices have been proposed and analysed. The permeability k can be determined using:

- indirect methods, by tests of stress relaxation or creep, in confined and unconfined configurations, obtaining then k, using a theoretical model or by curve-fitting the creep or relaxation curve generated in the experiments;
- direct methods, based on the measurements of the pressure drop and the volu-

metric flow of fluid through the material whose k has to be measured, by applying Darcy's law (Eq. 2.1).

Specifically, very few studies were aimed at investigating the hydraulic permeability of the brain, and practically none have also experimentally investigated the anisotropic behaviour of the WM and GM.

In fact, only [Franceschini et al., 2006] and [Tavner et al., 2016] experimentally studied this parameter, but the experiments were carried out at the macroscale on large samples (30 mm/5-8 mm initial diameter/height) and did not consider the microscale localised heterogeneities in the tissue. More importantly, they did take into account neither the anisotropy of brain tissue, because of the directionality of axons in WM, nor the effect of time post-mortem on k.

Materials and methods

Cylindrical specimens (5 mm/7 mm initial diameter/height) of ovine corona radiata were harvested from brains within 24 hours post-mortem. The samples were obtained from sagittal or coronal cut slices, using surgical scalpels and blades, and placed in a plastic tube (pipette), avoiding deformations of the tissue. The sagittal and coronal cuts allowed obtaining samples with parallel ($S_{\parallel}$) and perpendicular ($S_{\perp}$) fibres with respect to the cross-section area of the small tube.

Subsequently, each sample was placed into a glass bath, completely filled with PBS. A 30 gauge needle was inserted for about 3 mm into the sample. The applied pressure was held at 7 $mmHg$ for a period of 25-30 minutes to allow the brain sample to acclimatise to the pressure environment. After acclimatisation, an eight-step perfusion protocol was carried out, consisting of applied pressures of 10, 12.5, 15, 17.5, 20, 22.5 and 25 $mmHg$. The duration of each experiment was 2 hours. However, in some cases, a specimen could suffer abrupt disruption due to the big flow rate across the tissue or some imperfections inside the sample. The resulting flow rate, measured by the flow sensor, and the pressure drop across the sample, were used to calculate k.

Results and discussion

The analysis of the data was conducted considering different parameters: the effect of

the directionality of axons on the flow across the tissue, the effect of pressure on flow rate and k, and finally, the effect of post-mortem time on k.

For $S_{\parallel}$, the flow rate rises with increasing applied pressure from about 128 nl/min at 7 $mmHg$ to about 558 nl/min at 25 $mmHg$. However, for the same set of applied pressure steps, the flow rate across $S_{\perp}$ is much lower and rises from about 7 nl/min at 7 $mmHg$ to about 27 nl/min at 25 $mmHg$. The emerging differences between the two samples are due to the fact that the flow across the tissue is strongly dependent on the porous media structure which offers a very different resistance depending on the flow direction.

Moreover, in case of $S_{\parallel}$, when the axons are aligned to the injection direction, k is higher, while in case of $S_{\perp}$, the axons are perpendicular to the fluid, k is lower.

Finally, an analysis of the effect of post-mortem on k was conducted considering four different groups, divided by the direction of the fibres inside the tube (Parallel or Perpendicular) and by the time post-mortem, choosing as critical time 6 h post-mortem, as reported in literature by [Garo et al., 2007]: Parallel$\leq$6 h, Parallel>6 h, Perpendicular$\leq$6 h, Perpendicular>6 h, demonstrating a statistical difference of the respective permeabilities ($S_{\parallel}$ $\leq$6 h = 4.03×10^{-16} m^2; $S_{\parallel}$ >6 h = 4.48×10^{-16} m^2; $S_{\perp}$ $\leq$6 h = 0.812×10^{-16} m^2; $S_{\perp}$ >6 h = 0.881×10^{-16} m^2).

However, from the results obtained from this study, the authors concluded the permeability of both $S_{\parallel}$ and $S_{\perp}$ does not change within the 9 h post-mortem, but 24 h post-mortem resulted in the important threshold time, after which a significant difference in k is visible.

Conclusions

These results demonstrated that hydraulic permeability is significantly higher when the axons in WM are parallel to the flow direction in comparison to that when they are perpendicular to the flow direction. The tissue with axons parallel to flow is more vulnerable to sustain high pressures in contrast to the perpendicular axons which firmly sustain high pressures. Furthermore, the post-mortem time up to 9 h does not change the hydraulic permeability, however, 24 h post-mortem time makes the tissue more

permeable. These experimental results not only provide a valuable addition to address the issues in technologies like CED but also provide solid information which can be used to develop a detailed mechanical model for brain tissue.

Sommario

Introduzione

Il glioblastoma multiforme (GBM) è uno dei tumori cerebrali umani più frequenti e maligni, infatti presenta un tasso di sopravvivenza molto basso. Il piano di trattamento convenzionale prevede un intervento chirurgico, con il quale è praticamente impossibile rimuovere tutto il tumore, seguito da radiazioni e/o chemioterapia che, nel complesso, danneggiano il tessuto favorendo la tossicità sistemica.

Purtroppo, questi sistemi di somministrazione dei farmaci devono attraversare la barriera emato-encefalica implicando tutte le sue limitazioni circa la distribuzione del farmaco (dimensioni della molecola, polarità, specificità del substrato, meccanismi attivi di efflusso): ciò significa che i farmaci non raggiungono mai la regione target.

Dal 1994 è stata introdotta una nuova tecnica per bypassare la barriera emato-encefalica, ovvero la procedura chirurgica nota come CED (convection-enhanced delivery), con risultati promettenti. Con questo metodo, le chemioterapie intra-tumorali vengono somministrate per iniezione diretta sotto pressione positiva direttamente nel parenchima. Come suggerisce il nome, la convezione è utilizzata per integrare la diffusione e per introdurre molecole grandi e piccole. Tuttavia, l'efficacia di questa tecnica innovativa è legata alla capacità di garantire una sufficiente concentrazione del farmaco nella regione target. La concentrazione del farmaco è indipendente dalla velocità e dalla durata dell'infusione. La sua distribuzione è estremamente correlata alla regione in cui è infuso; una struttura omogenea o una struttura contenente fibre mostra differenti

vie di flusso. Diversi fattori contribuiscono al buon successo di questo trattamento e, in realtà, rigorosi modelli computazionali rappresentano un importante supporto. Tuttavia, parametri realistici sono necessari per implementare un modello numerico accurato e affidabile che includa l'orientamento dei tratti di fibre di materia bianca e i corretti tensori di permeabilità e diffusione. La determinazione di valori affidabili di permeabilità idraulica è ancora un attuale oggetto di ricerca, ma è un argomento di profondo interesse per il materiale biologico, a causa del suo importante ruolo in una serie di terapie basate sulla somministrazione di farmaci. La forte dipendenza della permeabilità dalla geometria e dalla topologia della struttura dei pori, e la mancanza di una conoscenza dettagliata di questi parametri nel caso del tessuto cerebrale, rende lo studio molto più impegnativo. Sebbene siano stati sviluppati modelli teorici per la permeabilità idraulica, l'evidenza sperimentale a completamento di questi modelli è carente o ancora in discussione.

Scopo del lavoro

Nel presente studio, gli autori hanno misurato la permeabilità della materia bianca del tessuto cerebrale ovino fresco considerando le eterogeneità localizzate nel mezzo utilizzando un impianto sperimentale basato sull'infusione, *iPerfusion*. È stata misurata la portata attraverso diverse zone della materia bianca in risposta alle pressioni applicate in campioni di dimensioni specifiche, ed è stata calcolata la permeabilità dai parametri misurati in modo diretto. Inoltre, è stato analizzato l'effetto dell'anisotropia del tessuto sulla permeabilità, considerando la direzionalità degli assoni, ed è stato anche verificato se la permeabilità idraulica della materia bianca cambiasse con il tempo post-mortem.

Stato dell'arte

In letteratura, molti studi affrontano la permeabilità idraulica dei mezzi porosi e, in particolare, diversi dispositivi di analisi dei tessuti molli sono stati proposti e analizzati. La permeabilità k può essere determinata utilizzando:

- metodi indiretti, mediante prove di stress relaxation o creep, in configurazioni confinate e non confinate, ottenendo poi k tramite un modello teorico o adattando, con un fitting, la curva di stress relaxation o creep generata negli esperi-

menti;

- metodi diretti, basati sulla misurazione della caduta di pressione e della portata del fluido attraverso il materiale da studiare, applicando la legge di Darcy (2.1).

In particolare, pochissimi studi sono stati finalizzati allo studio della permeabilità idraulica del cervello, e praticamente nessuno ha anche analizzato sperimentalmente il comportamento anisotropo della materia bianca e grigia. Infatti, solo [Franceschini et al., 2006] e [Tavner et al., 2016] hanno studiato sperimentalmente questo parametro, ma gli esperimenti sono stati condotti sulla macroscala e su grandi campioni (30 mm/5-8 mm di diametro/altezza iniziale) e non considerano le eterogeneità localizzate sulla microscala nel tessuto. Ancora più importante, essi non hanno mai preso in considerazione né l'anisotropia nella materia bianca, né l'effetto del tempo post-mortem.

Materiali e metodi

Campioni cilindrici (5 mm/7 mm di diametro/altezza iniziale) di corona radiata ovina sono stati prelevati dai cervelli entro le 24 ore post-mortem.

I campioni sono stati ottenuti da tagli sagittali e coronali, utilizzando bisturi e lame chirurgiche, e inseriti in tubi di plastica (pipette), evitando anche minime deformazioni del tessuto. In questo modo sono stati ottenuti entrambi i campioni con fibre parallele e perpendicolari, rispetto alla sezione trasversale del tubicino.

Successivamente i campioni, posti in un contenitore di vetro, completamente riempito di PBS, erano pronti per la perfusione dopo che un ago con un diametro di 30 gauge veniva inserito per circa 3 mm. La pressione applicata è stata mantenuta a 7 $mmHg$ per un periodo di 25-30 minuti per consentire al campione di acclimatarsi all'ambiente di pressione. Dopo questa fase iniziale è stato effettuato un protocollo di perfusione di otto fasi, che consisteva in pressioni applicate di 10, 12.5, 15, 17.5, 20, 22.5 e 25 $mmHg$. La durata di ogni esperimento è stata di circa 2 ore, ma, in alcuni casi, il campione ha subito una brusca interruzione a causa della grande portata attraverso il tessuto o di alcune imperfezioni all'interno del campione stesso. La portata risultante, misurata dal sensore di flusso, e la caduta di pressione attraverso il campione, leggermente inferiore alla pressione applicata, a causa della resistenza idrodinamica del sensore di flusso,

sono stati utilizzati per calcolare k.

Risultati e discussione

L'analisi dei dati è stata condotta considerando diversi parametri: l'effetto della direzionalità degli assoni sulla portata attraverso il tessuto, l'effetto della pressione sulla portata e su k, e, infine, l'effetto del tempo post-mortem su k. Per $S_{\parallel}$, la portata aumenta con l'aumento della pressione applicata da circa 128 nl/min a 7 $mmHg$ a circa 558 nl/min a 25 mmHg. Tuttavia, per lo stesso protocollo, la portata attraverso $S_{\perp}$ è molto più bassa e sale da circa 7 nl/min a 7 $mmHg$ a circa 27 nl/min a 25 $mmHg$. I campioni, con fibre parallele e perpendicolari, hanno profili simili, ma diversi quantitativamente. Ciò è dovuto al fatto che la portata attraverso il tessuto è fortemente dipendente dalla struttura porosa, che offre una resistenza molto diversa a seconda della direzione della portata.

Inoltre, nel caso di $S_{\parallel}$, quando gli assoni sono allineati alla direzione di iniezione, k è maggiore, mentre nel caso di $S_{\perp}$, con gli assoni perpendicolari alla direzione di scorrimento del fluido, k è minore.

Infine, seguendo la letteratura, è stata condotta un'analisi dell'effetto post-mortem su k, considerando quattro diversi gruppi, Parallel$\leq$6 h, Parallel>6 h, Perpendicular$\leq$6 h, Perpendicular>6 h, dimostrando una differenza statistica delle rispettive permeabilità ($S_{\parallel}$ $\leq$6 h = 4.03×10^{-16} m^2; $S_{\parallel}$ >6 h = 4.48×10^{-16} m^2; $S_{\perp}$ $\leq$6 h = 0.812×10^{-16} m^2; $S_{\perp}$ >6 h = 0.881×10^{-16} m^2).

Tuttavia, dai risultati ottenuti da questo studio, gli autori hanno concluso che la permeabilità di $S_{\parallel}$ e $S_{\perp}$ non cambia entro le 9 ore post-mortem, ma, la soglia di tempo dopo la quale è stata visibile una significativa differenza di k, è risultata spostata dopo le 24 ore post-mortem.

Conclusioni

Questi risultati hanno dimostrato che la permeabilità idraulica è significativamente più elevata quando gli assoni nella materia bianca sono paralleli alla direzione del flusso, rispetto a quando sono perpendicolari ad essa. Il tessuto con gli assoni paralleli al flusso è più vulnerabile e non adatto a sostenere pressioni elevate, diversamente a quando

presenta gli assoni perpendicolari, sostenendo saldamente le alte pressioni. Inoltre, il tempo post-mortem fino a 9 ore non modifica la permeabilità idraulica, mentre dopo le 24 ore post-mortem il tessuto risulta più permeabile. Questi risultati sperimentali non solo rappresentano un valore aggiunto per affrontare i problemi delle nuove tecniche come la CED, ma forniscono anche informazioni solide che possono essere utilizzate per sviluppare un modello meccanico dettagliato per il tessuto cerebrale.

Contents

List of Figures

List of Tables

Chapter 1

INTRODUCTION

In this chapter, the general framework where this thesis work is inserted will be presented. In Sec. 1.1 gliomas (glioblastomas, in particular) will be introduced from a clinical point of view, underling current criticalities. In Sec. 1.2 conventional treatments and their limitations will be described and in Sec. 1.3 particular attention will be paid on CED.

1.1 Clinical problem: Glioblastoma Multiforme (GBM)

Glioblastoma multiforme (GBM), a World Health Organization (WHO) grade IV glioma, is the most aggressive and common form of primary central nervous system (CNS) cancer in older adults [Wilson et al., 2014] (Fig. 1.1). A tumour grade is a way to classify a tumour in order to identify its general characteristics, determine treatment options, and predict outcomes. WHO brain tumour grading system classifies Grade I, II, III and IV, from a benign form of cancer, characterised by slow diffusion of the cells and long-term survival, to the most malignant tumour that ensures only a few months of survival (Tab. 1.1).

Current gliomas grading scale was updated on 2007 WHO, the widest accepted system, and it separates gliomas considering the cytologic features and their malignancy.

Table 1.1: *World Health Organization (WHO) brain tumour grading system.*

Grade	*Descriptions*
Grade I tumor	• Benign • Slow growing • Cells look almost normal under a microscope • Usually associated with long-term survival • Least likely to recur • Rare in adults
Grade II tumor	• Relatively slow growing (no mitosis) • Cells look slightly abnormal under a microscope • No vascular proliferation and no necrosis • Sometimes spreads to nearby normal tissue and can recur as a higher-grade tumour
Grade III tumor	• Malignant • Actively reproduces abnormal cells with a high rate of mitosis • Cells look abnormal under a microscope • No vascular proliferation and no necrosis • Often spreads into nearby normal parts of the brain and tends to recur
Grade IV tumor	• Most malignant • Grows fast with a very high rate of mitosis • Cells look very abnormal under a microscope • Presence of vascular proliferation and necrosis • Easily spreads into nearby normal parts of the brain

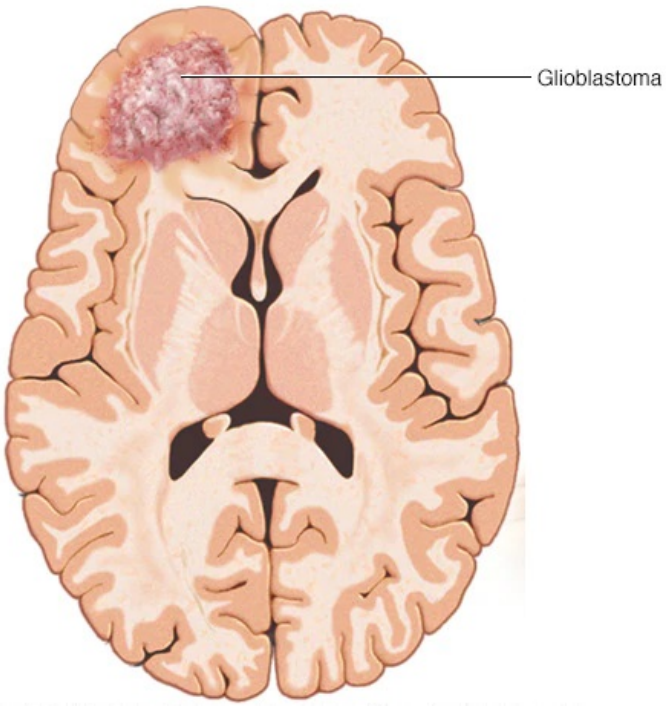

Figure 1.1: *Image of Glioblastoma Multiforme. From the anatomic-pathological point of view, the tumour appears as a mass of consistency and color different from the cerebral parenchyma. Source: Mayoclinic.org (available at: https://www.mayoclinic.org/diseases-conditions/glioblastoma/cdc-20350148)*

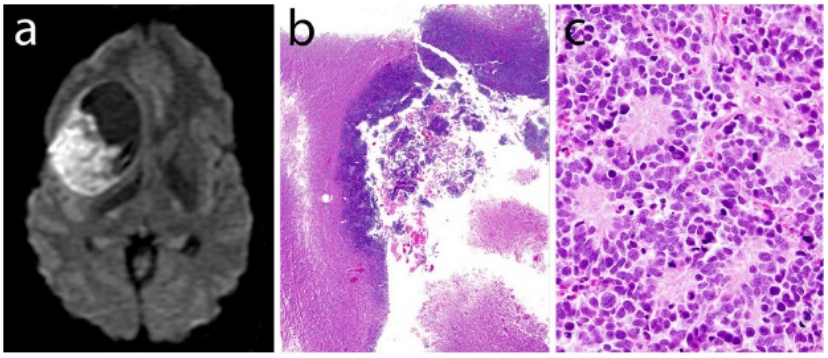

Figure 1.2: *Glioblastoma with primitive neuronal components (GBM-PNC). (a) In this Diffusion-weighted magnetic resonance image (DW-MRI) the restricted diffusion shows the more cellular primitive component. (b) The primitive clone in this GBM-PNC is evident as a highly cellular nodule within an otherwise classic diffuse astrocytoma. (c) Well-formed Homer Wright rosettes, nodules containing primitive cells that display neuronal differentiation, were seen in the primitive portion of this GBM-PNC. Image courtesy of [Louis et al., 2016].*

In fact, gliomas are tumours that originate from precursors of glial cells and so, according to their origin, they are also classified in astrocytoma (from astrocytes), oligo-

Table 1.2: *World Health Organization (WHO) classification for diffuse glioma.*

Type	*WHO Grade*	*Description*	*Median Survival* (Years)
Astrocytoma	II	Infiltrating tumour with increased hypercellularity	6-8
Oligodendroglioma	II	Occur in the white matter and cortex of the cerebral hemisphere	12
Oligoastrocytoma	II	Diffuse mixed tumour	3 to > 10
Anaplastic-astrocytoma Oligodendroglioma	III	Highly infiltrating tumours with increased mitotic activity	3
Glioblastoma	IV	Infiltrating glial neoplasm with necrosis and micro-vascular proliferation	1 to 2

dendroglioma (from oligodendrocytes), ependymoma (from ependymal cells), mixed glioma [Ostrom et al., 2013]. Combining these classification schemes, the resultant glioma classification is based on the type of the glioma and its grade, specifying its peculiarities and the survival rate (Tab. 1.2).

GBMs are also classified by the presence of precursors cells that caused the development of the cancer. They are divided into GBM IDH-wildtype, defined primary and GBM IDH-mutant, which correspond to so-called secondary [Louis et al., 2016]. Specifically, a primary GBM grows without malignant precursors, whereas secondary GBM is always related to a previous low-grade diffuse astrocytoma or anaplastic astrocytoma (Fig. 1.2).

Moreover, primary GBM is common and affects principally older patients (median age is 55 years); instead, secondary GBM affects patients with a mean age of 40 years old and it is characterised by a better prognosis thus leading to greater survival time [Wilson et al., 2014].

Finally, it is possible to outline four GBM subtypes, classical, mesenchymal, proneural and neural, based upon different genetic alterations. This analysis is possible thanks

to the high dimensional genomic profiling with which patterns of gene expression are established to identify the respective subtypes [Wilson et al., 2014].

GBMs are the most aggressive astrocytic tumour, showing the same mitotic activity of anaplastic lesions and causing necrosis and haemorrhage in the primal site. Its intrafascicular diffusion hinders the complete resection and excision of the tumour mass. Tumour cells have tentacle-like structures which spread very fast, leading to disease growing also far from the primary tumour [Vigneswaran et al., 2015][Wilson et al., 2014]. Recent studies conducted by [Mohsen et al., 2013], introduced a method to investigate the spreading of the tumour cells in the surrounding white matter (WM) tracts. Indeed, using diffusion tensor imaging (DTI)[1], patterns of a tumour recurrence are identified, allowing to a sort of prediction of sites of tumour progression. This evaluation is possible analysing the diffusivity of water protons in the tissue: it decreases when the extracellular part is composed by obstacles arranged in random position, while it increases when the obstacles are positioned in an organised way and also when that compartment is full of fluid, allowing the individualization of necrosis zone. By decomposing of the tensor into isotropic and anisotropic components, it is possible to differentiate the tumour from the healthy tissue (Fig. 1.3).

A recent statistical report by [Ostrom et al., 2013] highlighted that in primary brain and CNS tumours diagnosed in the United States in 2000-2010, the incidence rate of GBMs per 100.000 population/year was 3.97 in males and 2.53 in females. GBMs developed principally in older patients (mean age 64) because the incidence raises as the age increases [Ostrom et al., 2013].

In this dramatic scenario, GBMs remain incurable in most cases, leaving patients a median overall survival rate ranging from 12 to 18 months [Mehta et al., 2015].

[1]DTI is an imaging technique based on the measure of the diffusion of water molecules. It is used properly for imaging the white matter of the brain and it is applied to numerous scientific studies and clinical problems [O'Donnell and Westin, 2011].

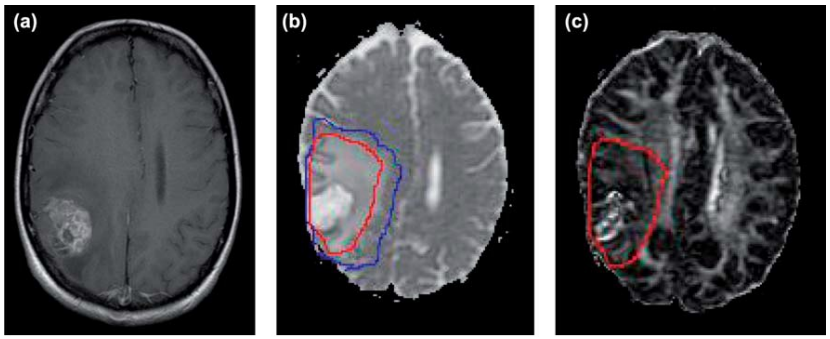

Figure 1.3: *The method proposed by [Mohsen et al., 2013] consists of the analysis of the progression of glioblastoma (GBM) with diffusion tensor imaging (DTI). In this way it is possible to predict the tumour extension, using different patterns previously reported to correlate to histo-pathological evidence of the tumour infiltration. This image shows a case of Diffuse Invasive pattern. (a) Post-contrast T1-weighted image shows a GBM in the right parieto-occipital region, surrounded by necrotic zones. (b) p-component of the tensor information with the isotropic region of interest (ROI) (blue) and anisotropic ROI (red). (c) q-component of the tensor information showing the distorted white matter (WM) tract due to the presence of the gross tumour abnormality. Image courtesy of [Mohsen et al., 2013].*

1.2 Conventional treatments and limitations

There are many types of cancer treatments. GBMs are treated with maximal safe resection, followed by radiation therapy (RT) and chemotherapy (with temozolomide (TMZ)) as the standard of care [Wilson et al., 2014].

- **Maximum surgical resection** is the first solution to standard care, paying attention to preserve neurologic functions. Moreover, nowadays there are some image-guided surgical techniques that assist the surgery, such as intraoperative magnetic resonance imaging (MRI), cortical mapping and stereotactic surgery. The last innovative modality is the fluorescence guidance, allowing direct visualization of tumour borders [Anton et al., 2012][Stummer et al., 2006].

- **Radiation Therapy** consists of a high dose of focal radiations that kill cancer cells, damaging their DNA and inducing synergic cytotoxicity. It usually follows the surgical treatment.

- **Chemotherapy** uses drugs to stop cancer cells from reproducing, avoiding their spreading in the body. It should be intravenous or oral. Unfortunately, it includes

a long list of side effects, such as feeling tired most of the time, feeling sick and vomiting, hair loss, increasing risk of picking up infections, dry or itchy skin, diarrhoea or constipation [Pearce et al., 2017].

- Recently, **chemoradiotherapy** has become a standard adjuvant postoperative therapy. It consists of the combination of RT and TMZ and it prolongs the median survival time [Stupp et al., 2005]. Specifically, this treatment includes 6 weeks of RT and TMZ, followed by 6 cycles of TMZ. RT is a focal technique, delivered with linear accelerators for a total dose of 60 Gy and used with concomitant chemotherapy. Later, patients receive a 150 $mg/m^2/day$ of TMZ for 5 days every 28 days for at least 6 cycles [Stupp et al., 2005].

Unfortunately, due to the strongness of the GBM cells, all these current therapies are unsuccessful to eliminate the tumour [Zhou et al., 2013]. The principal reason is the blood-brain barrier (BBB). It is a diffusion barrier, which isolates the brain from the rest of the body and maintains brain homeostasis. For these reasons the BBB blocks most of the anticancer drugs in the blood retarding the drug penetration and accumulation in the target region [Alam et al., 2010][Zhou et al., 2013].

1.3 Innovative treatment: Convection-Enhanced Delivery (CED)

Neurosurgical community proposed for recurrent GBM multiple modes of intratumoral therapy, such as instillation of chemotherapy, nanoparticles, gene therapy, interstitial wafer chemotherapy, tumour-treating fields, and convection-enhanced delivery (CED) [Sampson et al., 2011][Quinn et al., 2009][Kirson et al., 2007][Kirson et al., 2009] [Lidar et al., 2004][Brem et al., 1995][Engelhard, 2000]. Among all these alternatives, a promising technique, (in particular for GBM patients [Mehta et al., 2015]), which has been introduced by [Bobo et al., 1994], is CED. This method consists of an infusion of drugs, under positive pressure gradient, directly into the CNS parenchyma. In this way, a bulk flow supports simple diffusion [Bobo et al., 1994] thus obtaining a wider

spreading of the drug. Previous studies demonstrated that CED is a homogeneous, safe and targeted way to transport small- and large-molecular weight infusate in the parenchyma [Morrison et al., 1994][Muldoon et al., 1995].
However, this alternative delivery system must be optimised since its efficacy is related to the ability to obtain a sufficiently high concentration of drug in the targeted region [Mehta et al., 2015]. Several variables contribute to the success of this technique, in particular the appropriate rate of infusate delivery, the correct concentration of infusate, and an optimal position of the catheter [Chen et al., 1999]. Moreover, also the effectiveness to obtain a sufficient high concentration of the drug in the targeted region [Mehta et al., 2015] and its ability to predict, in the pre-operative phase, the distribution of the drug inside the tumour [Raghavan et al., 2016] are essential factors to be taken into consideration. For example, tissue anisotropy of the brain plays a key role for drug distribution and a better understanding can improve the prediction of computational models, allowing CED treatments as an approach for GBMs intratumoral therapy [Mehta et al., 2015]. This aspect of the brain can be defined by a scientific parameter, the hydraulic permeability, defined as the measure of the flow resistance, which is exerted by the solid matrix (cells, extracellular matrix). It depends on the geometry and the size of the pore structure [Kapellos and Alexiou, 2013].

1.4 Aim of the work

This thesis aims to present an experimental work that demonstrates the anisotropic behaviour of the hydraulic permeability in the WM of the brain. In fact, the determination of the hydraulic permeability of the brain is still a subject of current research. There are several theoretical values for permeability in literature, however they vary up to three orders of magnitude [Chatelin et al., 2010] and therefore a detailed investigation is needed.
In the present study, fresh ovine brain was used and experiments were performed to determine the localised hydraulic permeability of WM using an infusion-based experimental set up, *iPerfusion* [Sherwood et al., 2016]. The flow across a specific part of WM in response to applied pressures for a sample of specific dimensions was measured

and the permeability from directly measured parameters was calculated. Furthermore, it was explored if the hydraulic permeability of WM changes with post-mortem time. It was also investigated the effect of anisotropy of WM on the hydraulic permeability and to the best of authors' knowledge, this is a first experimental study reporting the effect of directionality of axons on the hydraulic permeability of white matter.

This thesis is developed within the framework of EDEN2020 (Enhanced Delivery Ecosystem for Neurosurgery in 2020), a European project led by Imperial College London, where the thesis was partially developed.

Chapter 2

STATE OF THE ART

This chapter represents a literature review about the methods of hydraulic permeability measurements. After a brief introduction of the the anatomy of the brain, the Sec. 2.1 introduces direct and indirect methods of permeability, analysing the experimental set-up for soft tissues. Moreover, a state of the art of the experiments on brain tissue will be discussed. Finally, the limitations of the state of the art will be exposed in Sec. 2.2.

The brain is one of the most complex organs. It is positioned in the cranial cavity and it is connected to the spinal cord. Together, they are the principal centres of integration of information of the Central Nervous System (CNS). At a microscopic level, the CNS is primarily a network of two kinds of nervous tissue, white and grey. The white nervous tissue (WM) consists of axons, whereas the grey nervous tissue (GM) consists mainly of nerve-cell bodies, embedded in neuroglia, which covers the surfaces of the brain and some deep zones within the brain [Snell, 2010].
An in-depth study of the anatomy of the brain is explained in the Appendix A.

2.1 Methods of permeability measurement

The brain is a porous media, in which the fluid moves in the extracellular space, among the cells. A fundamental parameter to indicate the ease of fluid flow through a porous

material is the "hydraulic permeability" [Gu et al., 1999]. Although several mathematical definitions for the hydraulic permeability coefficient k exist in the literature, Darcy's law was adopted for this study:

$$\vec{v} = \frac{k}{\mu} \cdot \nabla P \tag{2.1}$$

where μ is the viscosity of the fluid, $\vec{v}$ is obtained by the ratio of Q (the volumetric flow rate (volume per unit of time)) to A (the permeation area of the sample), ∇P is the pressure drop across the thickness of the sample ($\frac{\Delta p}{L}$).
Darcy's law is valid only when the following conditions exist [Burmister, 1955]:

- the flow is laminar;
- steady-state conditions are present;
- voids are saturated;
- continuity conditions are satisfied and no volume change occurs during or as a result of the flow.

In the literature, a huge number of studies faces the hydraulic permeability of the porous media but in this thesis, the authors will limit to explain, in a detailed way, only the principal methods relevant for the soft tissues. This is related to the fact that the brain, the object of the analysis of the study, is part of this category. The interest in the knowledge of the measure of the ease with which fluid can flow through this kind of tissue is strictly connected to its fundamental role in the biorheological functioning [Holmes, 1985], influencing cell nutrition and tissue viscoelastic behaviour [Mow et al., 1980][Mow et al., 1998][Holm et al., 1981][Setton et al., 1993][Urban et al., 1977]. Several soft tissue permeability testing devices have been reported in the literature, including all the studied tissues e.g. cartilage [Mow et al., 1984], corneal endothelium [Fischbarg et al., 1980], vascular tissue [Isogai et al., 1983], lipid bilayers [Nagle and Scott, 1978], mucus [Katz et al., 1982], red cell membranes [Mlekoday, 1983], nucleus pulposus [Heneghan and Riches, 2008] and annulus fibrosus [Gu et al., 1999][Gu and Yao, 2003], but also food tissue [Datta, 2006], tumoural tissue [Zhang et al., 2000], tissue-engineered [Vunjak-Novakovic et al., 1999], scaffold [O'Brien et al.,

2006], and gels [Andriakopoulou et al., 2018] that mimic the same characteristics of the soft tissues. The greatest difficulties related to this kind of tissue are the extremely low velocities involved, and the deformation of the solid matrix induced by the flow [Mansour and Mow, 1976][Barry and Aldis, 1990]. The hydraulic permeability can be investigated through **direct** and **indirect** methods. Direct methods are based on the measurement of the pressure drop and the volumetric flow of fluid through the material whose permeability has to be measured [Pennella et al., 2013]. A number of methodologies for assessing the flow rate has been reported in the literature and they are grouped into pump-based method, falling head method, constant head method. For each method, a relevant experiment on the soft tissues will be analysed and described.

- **Pump-based method**: it implicates a fluid motion, generated by a pump, through a sample. In particular, in case of very low flow rates, a syringe pump is usually used [Sherwood et al., 2016]. The simplest pump-based approach consists in generating a controlled flow rate, and measuring the pressure drops across the sample. Several researches used this approach, developing a pressure-induced permeability test to assess the permeability of scaffolds made of different kinds of materials [Ochoa et al., 2009][Truscello et al., 2012][Santamaría et al., 2012][Swider et al., 2007][Shimko and Nauman, 2007][Innocentini et al., 2010][Chor and Li, 2007][Schiavi et al., 2012][Wang et al., 2010]. This technique presents several advantages e.g. simplicity to perform, but it also has a few drawbacks which might be difficult to deal with, such as the selection of steady-state, that is not clearly defined [Sherwood et al., 2016] and this may take a very long time (as shows [Kumar et al., 2013] in their study, to measure the outflow facility during the eye perfusion).

  One of the most interesting experiments with this kind of technique using soft tissues was conducted by [Weiss and Maakestad, 2006]. In 2004 they studied the apparent and intrinsic permeability of the human medial collateral ligament (MCL), exploiting a transversal flux to the direction of the collagen fibres. They designed a custom permeation apparatus to apply a small flow rate into cylindrical ligament specimens, monitoring the resultant gradient of pressure. MCLs

were harvested from 5 human knees and the permeability measurements were performed at 3 levels of compressive pre-strain (10%, 20%, 30%) and 5 pressures ($0.17, 0.34, 1.03, 1.72$ and 2.76 MPa). The apparent permeability was calculated with Darcy's law, whereas the intrinsic permeability was obtained as a function of applied compressive pre-strain only. A syringe pump (SP-10li, WPI, Sarasota, FL) was used with a 500 μl glass syringe (Hamilton 1750, Reno, NV) to apply a constant flow rate ($0.001 - 100\ \mu l/min$). The resultant gradient of pressure was monitored continuously by a pressure transducer (Setra, Boxborough, MA, accuracy 0.004 MPa). The size of the area exposed to the flow was equal to 3 mm of diameter. A micrometer head (Newport, Irvine, CA, accuracy 1 μm) applied a uniaxial compression of pre-strain along the direction of permeation, compressing a porous filter against the superior part of the sample and an O-ring (Fig. 2.1).

The filter was made of polyethylene, relatively rigid (compressive modulus = 18.7 MPa), highly permeable (hydraulic permeability = $3 \cdot 10^{-10}\ m^4/Ns$), guaranteeing the flux through the sample; the O-ring sealed off the passage of flux outside the specimen. If on one hand small flow rates into small specimens are the positive aspects of the test, on the other hand, the filter around the sample is a barrier and experiments with pre-strains less than 10% and high pressures can cause separation of the sample from the filter.

- **Falling head method**: it is characterised by a small diameter (D) reservoir (called also standpipe), open to atmospheric pressure, which provides the water head, a permeability chamber and another reservoir for water collection [Pennella et al., 2013]. The sample is placed under the hydraulic head which decreases in magnitude with time as the fluid passes through the material and the level of the water in the reservoir goes down, over time t. Applying Darcy's law, after integration over the measured time interval $t - t_0$ (using $t_0 = 0$), the hydraulic permeability k of the material can be derived as:

$$k = \frac{aL}{At} \cdot ln\frac{H_1}{H_2} \cdot \frac{\mu}{\rho g} \tag{2.2}$$

where a is the cross-sectional area of the standpipe; L is the thickness of the

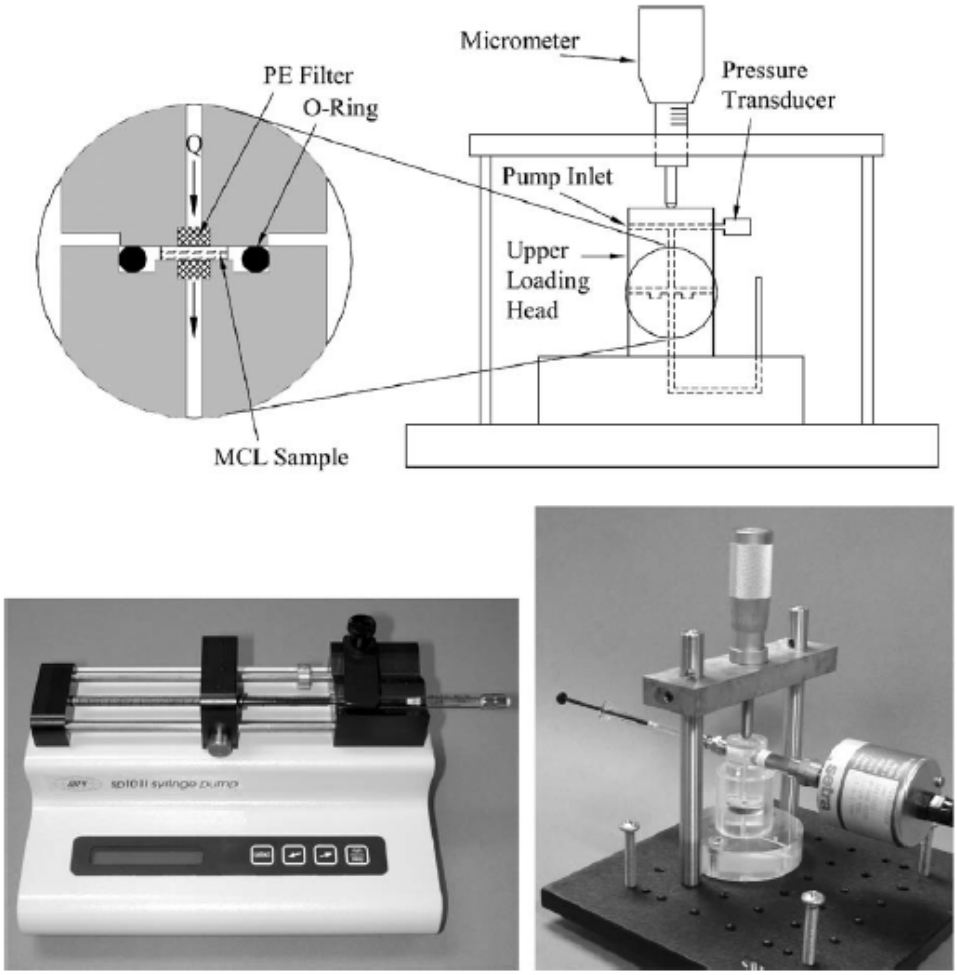

Figure 2.1: *Top - Schematic illustrating set-up and flow of fluid. Lower left panel - Syringe pump used for infusion at a user-adjustable flow rate. Lower right panel - Assembled permeation device. Glass syringe is in position for infusion. Picture courtesy of [Weiss and Maakestad, 2006].*

sample; A is the cross-sectional area of the sample under investigation; H_1, H_2 are the hydraulic heads at the start and end of the run. The advantages of this method are the ease of control of the water head (the flow rate is measured according to the change of mass [Barany, 1964] or the change in height [Aihara et al., 2003] of the fluid reservoir) and the insignificant effect of evaporation on the results. However, this approach becomes challenging with materials characterised by very low flow rates. In fact, instantaneous flow rates are not possible to measure, but only an average value over the evaluated period time is possible [Sherwood et al., 2016]. Since the standpipe is graduated and used to measure the head, there are two solutions to increase the resolution in the measurement

of the flow rate: the reduction of D of the standpipe or to extend the duration of the test. However, in both cases a significant variation in the applied pressure occurs [Sherwood et al., 2016]. Disadvantages are the greater complexity required, the possible effect of refilling the reservoir periodically, and the effect of the entrapped air on the calculated permeability because this method dissolves air less effectively in the percolating water [Fireman, 1944].

An innovative approach was used by [Zhang et al., 2000] who investigated the interstitial hydraulic permeability in a fibrosarcoma. Specifically, they used two experimental systems: the first one, more classic, concerns a one-dimensional perfusion through tumour slices, based on the design of [Swabb et al., 1974], opportunely modified; the second one, more innovative for this kind of measurements, regards an intratumoral infusion using a needle, involving a three-dimensional perfusion. If the perfusion system is very similar to the other devices, the intratumoral infusion deserves to be counted in this short but essential list of the state of the art of permeating apparatuses, classifying itself as a particular falling head method. Fibrosarcoma chunks (1 mm in diameter) were transplanted subcutaneously into hindlimbs of rats. When tumours reached 2-3 cm in diameter, it was removed, cut and put into cold Dulbecco's modified eagle medium (DMEM). The permeability measurements with intratumoral infusion were conducted as follows: a tumour chunk was immersed in physiological saline, maintained at 4°C, and perfused with the solution of 0.1% Evans blue-labeled albumin via a $23G$ needle. The needle was connected to an albumin solution reservoir, whose height defined the perfusion pressure. The flow rate was determined by the product of the velocity of a small air bubble, introduced into the tubing connecting to the reservoir, and the cross-sectional area of tubing. However, for this configuration, with pressures of 94 and 163 $cm\ H_2O$, the tumour chunks became blue within 10 min before the perfusion reached the steady-state. To overcome this problem, the flow rate was measured every 20 s until its variation was $<10\%$ between two adjacent measurements. Apparent permeability was calculated with Darcy's law for unidirectional flow in an infinite region around a spherical fluid cavity, at 20

and 36 $cm\ H_2O$, at steady-state of perfusion:

$$K_{\text{app}} = \frac{Q}{4\pi a_0 P_0} \tag{2.3}$$

where Q is the flow rate, P_0 is the perfusion pressure, and a_0 is the initial radius of the fluid cavity (assumed to be equal to the radius of needle tip). K_{app} was used to determine k, as a function of tissue deformation, with a mathematical model [Barry and Aldis, 1990][Huang et al., 1997][Klanchar and Tarbell, 1987][Lai and Mow, 1980][Parker et al., 1987]. Finally, the estimation of the distribution volume of Evans-blue-labeled albumin was done immediately after the intratumoral infusion. Tumour chunks were sectioned along the needle track and the shape of the blue region was approximately ellipsoid. Thus the volume was calculated as $3/(32\pi o_1 o_2 o_3)$, where the lengths of three axes (o_1, o_2 and o_3) of the ellipsoid were measured in tumour chunks using a pair of electronic calipers.

- **Constant head method**: it is generally based on a permeability test apparatus composed of a constant head reservoir and a large diameter outlet reservoir, to apply a constant pressure difference [Sherwood et al., 2016][Pennella et al., 2013]. So, the sample is subjected to a constant hydraulic potential and, typically, the average rate of flow is calculated based on the pressure drop along a capillary tube of known diameter, located upstream of the sample [Sherwood et al., 2016]. Considering Darcy's equation and assuming that Q represents the rate of flow per unit time; A, the cross-sectional area of the sample perpendicular to the flow direction; H, the total hydraulic head, and L the thickness of the sample:

$$k = \frac{QL}{AH} \cdot \frac{\mu}{\rho g} \tag{2.4}$$

It has the following advantages: the sample is not affected by any disturbances during the entire run, the fluid exiting from the sample is quickly and accurately measured and the equipment is easily available [Fireman, 1944]. Disadvantages of this method are the necessity to maintain a constant head and to the measure the pressure accurately. A small diameter capillary would be necessary, in order to generate an accurately measurable pressure drop (about 75 μm or less), but this kind of capillaries are subject to blockages and biofilm formation, which influence the hydrodynamic resistance of the tube and consequently the estimation

of the flow rate [Sherwood et al., 2016].

In 2006, [Reynaud and Quinn, 2006] studied both the axial hydraulic permeability of cartilaginous samples and the radial once, with a device which falls in this typology of method. This double measurement was possible thanks to two holes in the inferior part of the apparatus: the first one placed exactly under the specimen, to measure the axial permeability and the second one, positioned laterally, to acquire the radial permeability. Also in this case, an O-ring (see Fig. 2.2) functioned as a perfect gasket. The two holes were connected to two glass capillaries, from which it is possible to measure the flow rate. Differently from the previous experiments, here the reservoir in the upper part was a column of PBS in flexible silicone tubing (MasterFlux) and applied constant hydrostatic pressure to a 300 µm diameter region of the cartilage. A limitation is in the modality of bonding of the specimen because it does not ensure the elimination of secondary fluxes along the edges of the specimen, which will misrepresent the test. Different is the device designed by [O'Brien et al., 2006], which fills all the limits showed in the previous studies.

This test apparatus was used to measure the permeability of collagen-GAG scaffolds, but it is proved to be effective for all scaffold variants and for all levels of applied compressive strain. The mechanism by which the material is secured is innovative. It consists of two (top and bottom) brass plates with an 8 mm inner diameter tube, glued to two medical-grade stainless steel (Braun, Frankfurt, Germany) meshes (Fig. 2.3). The bottom mesh physically supports the scaffold whereas the upper one applies compressive strain to the scaffold via the height-adjustable top plate. Moreover, this arrangement also allowed various levels of compressive strain to be applied using spacers of varying thickness without severely distorting the scaffold. The scaffold edges were clamped in place, resulting in a secure boundary between the sample and walls of the device and the mesh did not inhibit or disrupt fluid flow through the apparatus. Like in [Reynaud and Quinn, 2006], a pressure is applied (the thickness of the spacers of $2.1, 2.5, 3$, and 5 mm with the thickness of the scaffold equal to 3.5 mm, create a compressive strain of 40%, 29%, 14%, and 0%, respectively) and the flow rate was

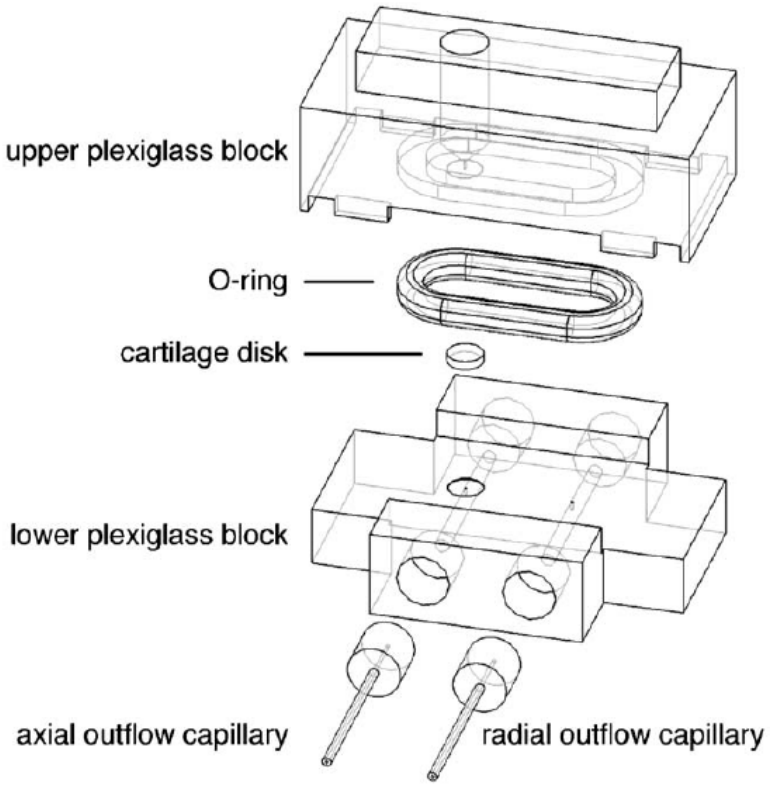

Figure 2.2: *Exploded view of the apparatus designed by Reynaud and Quinn. Cartilage disks were compressed between precision-machined plexiglass blocks. In the upper and bottom parts there are 300 μm diameter holes, which provided conduits for fluid flow. Picture courtesy of [Reynaud and Quinn, 2006].*

measured from the tube attached to the bottom plate of the permeability device using a stopwatch (Oregon Scientific, Portland, Oregon, USA) and an electronic scale accurate to within 0.05 g (Mettler Toledo, Greinfensee, Switzerland).

The permeability can be measured also indirectly by using properties of the material analysed, such as pore size and porosity of the medium, or by consolidation test [Fireman, 1944]. Specifically, there exist two experimental configurations: confined and unconfined tests. In a **confined test** the soft tissue sample is placed in a fluid-filled confinement chamber (Fig. 2.4 - Left side). The superficial zone is compressed by a rigid piston that can be porous or impermeable; the base is an impermeable or porous filter, respectively. In this way the radial flux and the radial deformation are prevented, and only the axial ones are allowed [Griffin et al., 2016]. From this compression test,

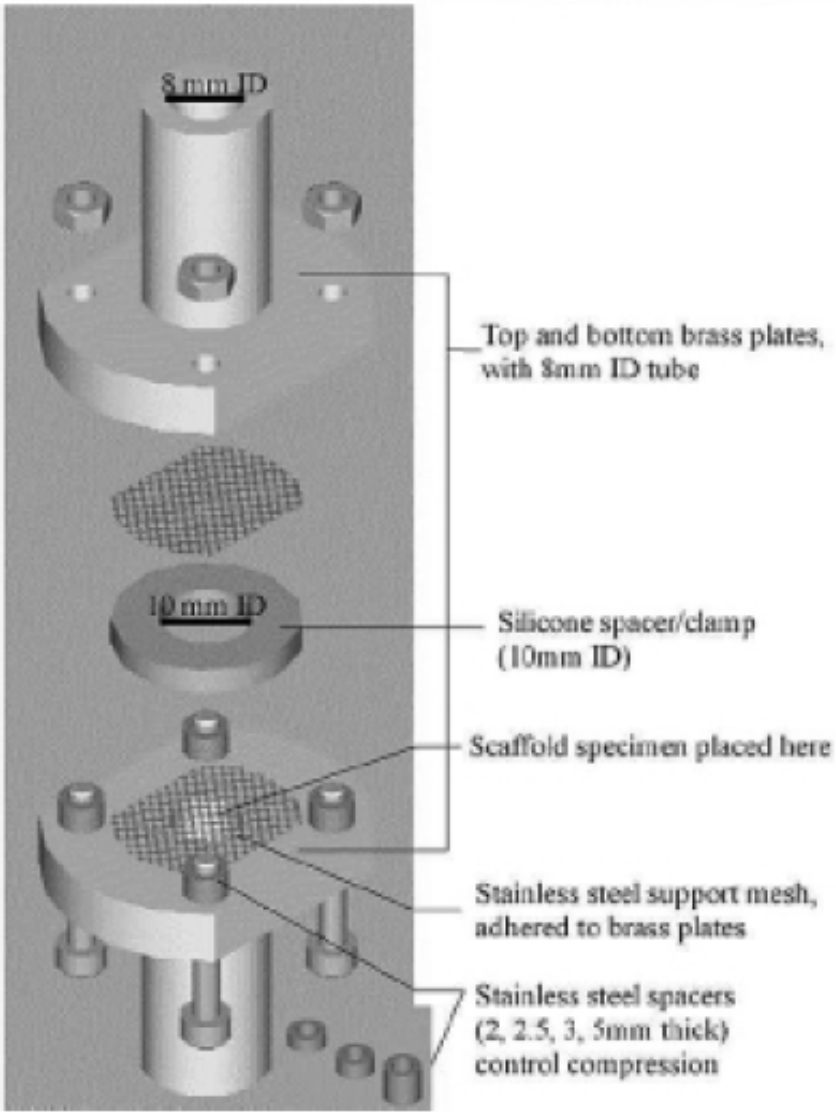

Figure 2.3: *The device made by O'Brien et al. The presence of the silicon spacers of different thickness allowed to apply different gradient pressure ensuring no fluid flow from the scaffold edges. Picture courtesy of [O'Brien et al., 2006].*

the aggregate modulus (H_{agg}), related to the deformation of the tissue, is directly calculated [Lu and Mow, 2008]. The **unconfined test** consists of a non-porous chamber (Fig. 2.4 - Right side) where the specimen is placed and it is loaded by a non-porous plate. Differently from the previous case, here only the radial flux is present [Griffin et al., 2016], and the parameters directly calculated are the Young modulus (E) and the Poisson's ratio (ν) [Lu and Mow, 2008]. In these confined and unconfined compression tests, the hydraulic permeability can be determined by curve-fitting the creep

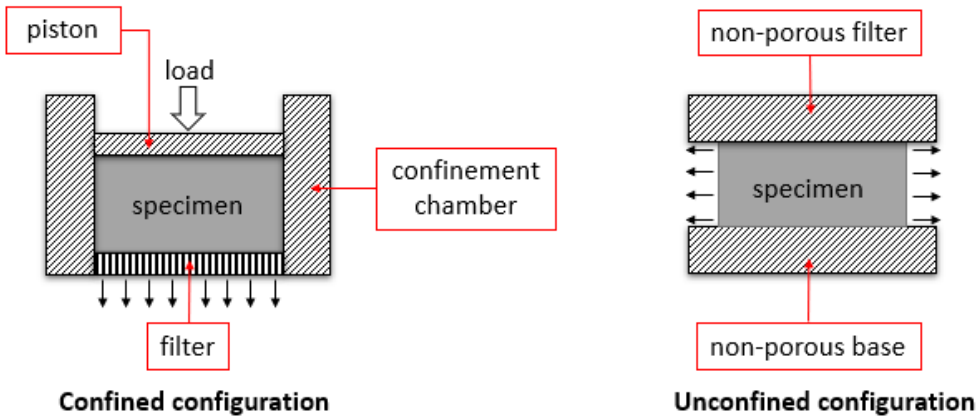

Figure 2.4: *Left - Confined configuration: the specimen is placed in an impervious chamber. Then the tissue is loaded through a porous (or impermeable, if the base is permeable) plate. Since the chamber is impervious, flow through the specimen is only in the vertical direction. Right - Unconfined configuration: the specimen is loaded using a non-porous filter onto a non-porous base, forcing the fluid flow to be predominantly radial.*

or relaxation curve generated in the experiments, in fact it requires apriori hyphoteses on the dynamic model of the tissue under investigation [Lu and Mow, 2008].

2.1.1 Experiments on brain tissue

The brain falls into the category of soft tissues and being the object of the study of this thesis, a separate section will be dedicated to the experiments on it.
The mechanical characterization of brain tissue has been the object of many studies for over 50 years. However, due to the extreme complexity of the soft tissue and the wide range of experimental methods and protocols that have been used for its characterization, the results described in the literature often differ by orders of magnitude [Chatelin et al., 2010] (Tab.2.1). Specifically, very few studies were aimed at investigating the hydraulic permeability of the brain, and practically none have also experimentally investigated the anisotropic behaviour of the WM and GM. The experiments conducted by [Reulen et al., 1977] show one of the first approaches that analyse the mechanism that happens through the WM, investigating the vasogenic type of brain edema. Their results were used from [Kaczmarek et al., 1997] to determine the permeability of the

WM and GM. Despite, a lot of studies investigated this parameter experimentally and computationally, suggesting also different parametrical models and still today it is the object of many scientific researches.
Even if, different testing protocols and monitoring of environmental and testing conditions may have led to the large disparity in results, to the best of authors' knowledge, only two studies have experimentally determined hydraulic permeability.

Franceschini et al., 2006

[Franceschini et al., 2006] conducted an extensive and comprehensive work in which they performed several types of mechanical tests on human brain samples within 12 h of death. Focusing on the permeability measurements, an oedometric test (Fig. 2.5) was performed on 12 cylindrical specimens harvested in the parietal lobe. The con-

Table 2.1: *Permeability, k, for brain tissue extracted from the literature, in chronological order. a) Theoretical approach; b) Experimental approach.*

k $[m^2]$	*Reference*	*Description*	*Typology of the study*
$7.5 \cdot 10^{-15}$ $5.0 \cdot 10^{-15}$	[Basser, 1992]	white matter grey matter	a)
$1.6 \cdot 10^{-14}$ $1.6 \cdot 10^{-16}$ $1.6 \cdot 10^{-15}$	[Kaczmarek et al., 1997]	white matter + grey matter + ependyma	a)
10^{-12} 10^{-15}	[Kalyanasundaram et al., 1997]	white matter grey matter	a)
$1.0 \cdot 10^{-13}$ $5.0 \cdot 10^{-15}$	[Miga et al., 2000]	white matter grey matter	a)
$4.87 \cdot 10^{-16}$	[Netti et al., 2000]	U87 glioblastoma	a)
$2.42 \cdot 10^{-17}$	[Franceschini et al., 2006]	human brain	b)
$4.08 \cdot 10^{-15}$	[Cheng and Bilston, 2007]	white matter	a)
$6.45 \cdot 10^{-15}$	[Arifin et al., 2009]	brain tissue	a)
$2.42 \cdot 10^{-17}$	[Tavner et al., 2016]	lamb brain	b)
$1.4 \cdot 10^{-16}$	[Vidotto et al., 2019]	brain tissue	a)

solidation ratio, obtained as the average ratio between the initial and final specimen's shortening under a loading step, was calculated as a function of time. These data were

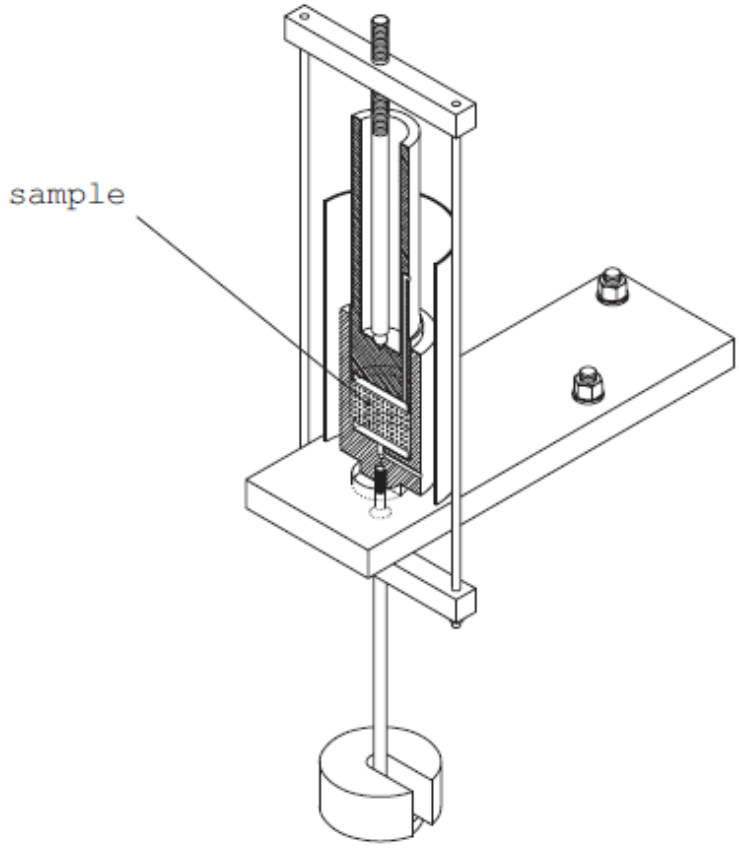

Figure 2.5: *A sketch of the oedometer used by Franceschini et al. It consists of a metallic mould, where the specimen is manually placed and then loaded through a cylindrical piston. Two filter paper are positioned between the sample and porous metal brass. Vertical displacement of the sample was recorded employing an LVDT connected to an electronic acquisition system. Picture courtesy of [Franceschini et al., 2006].*

fitted according to Terzaghi's theory thus allowing to infer the permeability. In the oedometric condition, the governing equation becomes:

$$c_{\mathrm{v}} \frac{\delta^2 p_{\mathrm{w}}}{\delta z^2} = \frac{p_{\mathrm{w}}}{\delta t} \tag{2.5}$$

where z is the space variables, t is the time variable, p_{w} is the pore fluid pressure, c_{v} is the coefficient of consolidation defined as:

$$c_{\mathrm{v}} = \frac{kM}{\gamma_{\mathrm{w}}} \tag{2.6}$$

where k is the permeability, M is the elastic oedometric coefficient and γ_w is the specific weight of the saturating fluid.

Two important limitations characterised this test: firstly, the permeability is not measured directly, but it is inferred from a model which is based on certain assumptions; secondly, the hydraulic permeability decreases with time post-mortem and its estimation is therefore affected by the exact time measurements have taken place [Tavner et al., 2016].

Tavner et al., 2016

[Tavner et al., 2016] carried out a series of simple experiments using lamb and sheep brain to establish the rate at which cerebrospinal fluid (CSF) moves through the brain parenchyma. The apparatus consists of a cylindrical die and a transparent plastic tube of length 85 cm. An O-ring placed into the die ensured sealing between these two elements, preventing any artificial CSF (ACSF) solution leakage; finally, a wire mesh was attached to the bottom of the die (Fig. 2.6).

Cylindrical samples (diameter 30 mm and height 20 mm) were cut from the brain (previously cleaned from pia mater) and inserted in the tube. The punch used to cut the sample had the same dimensions of the internal diameter of the die, in order to induce a negligible strain mounting the tissue within the die. The pressure was applied directly to the brain parenchyma by the column of artificial cerebrospinal fluid (ACSF), without deformation of the tissue. Three different heights ($10, 20, 85$ cm) were applied to the cylindrical specimen, each one for different periods, from 120 min to 20 h. For all these time periods no measurable change in the height of the ACSF solution column and no leakage of ACSF solution into the beaker through the brain tissue were observed. So a second set of experiments was carried out, using the same apparatus including a capillary tube filled with Toluidine Blue dye, above the ACSF column and a filter paper between the brain sample and the mesh. In this way also a very small quantity of liquid into the brain tissue was detected. After 23 h, under 20 cm of ACSF, the samples were immediately removed, frozen, sectioned and analysed under a microscope to estimate the depth of penetration of the toluidine blue dye. Even if neither in the beaker and on the filter paper there was no trace of the dye visible,

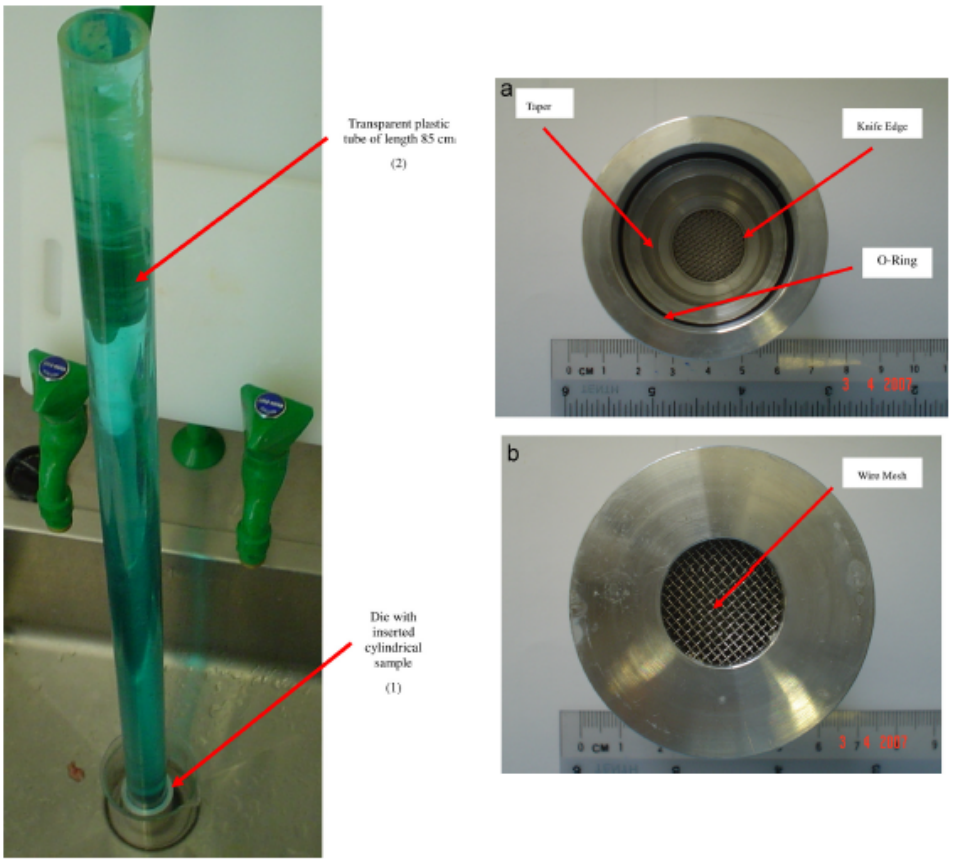

Figure 2.6: *Left - Experimental set-up created by Tavner et al. Here, 85 cm ACSF are applied on cylindrical sample inserted into the die. Right - Top (a) and bottom (b) view of the cylindrical die. Picture courtesy of [Tavner et al., 2016].*

movement of the ACSF column in the capillary tube indicated that ACSF was moving into the brain. Finally, the same experiments were also repeated adding in the ACSF 5 mg/l of PGMA polymer nano-particles (90 nm in diameter) with Rhodamine B attachments. Following the same procedure of the previous experiments and analysing the specimens under the microscope with green light, it was possible to see the depth of penetration of the particles. From this estimation the seepage velocity (v_{w}) into the brain is calculated, which is related to the flow rate (q):

$$q = v_{\mathrm{w}} \cdot s \cdot n \tag{2.7}$$

where s is the saturation (assumed as a high level) and n is the porosity (assumed equal to 0.2). The hydraulic conductivity was calculated as follows:

$$q = -k\frac{\delta\Phi}{\delta z} \quad with \quad \Phi = z + \frac{u_{\mathrm{w}}}{g\rho_{\mathrm{w}}} \tag{2.8}$$

where q is the volumetric flow rate, k is the hydraulic conductivity of the medium, Φ is the piezometric head, u_{w} is the pressure of wetting fluid, ρ_{w} is the density of the wetting fluid, z is the elevation above a datum and g is the magnitude of the gravitational acceleration which acts in the reverse z-direction. The main limitations of this work are the following: it has been omitted the analysis of the variation of the hydraulic conductivity related to a changing deformation because it is expected a reduction of the conductivity with a compressive strain; the experiments were carried out in-vitro but hydraulic conductivity decreases with increasing time post-mortem.

2.2 Limitations of the state of the art

As seen in the previous section (Sec. 2.1.1) only a few studies have experimentally determined hydraulic permeability, but their results are debatable because of the sample and experimental protocol adopted. Franceschini et al. [Franceschini et al., 2006] have done a uniaxial deformation in vitro experiment on human brain tissue excised within 12 h of death and have indirectly determined permeability from the compressibility parameters by fitting the data to Terzaghi's theory. Also Tavner et al. [Tavner et al., 2016] have used a perfusion experiment and have determined the hydraulic permeability of lamb and sheep brains using Darcy's law. However, both of these studies are carried out at macroscale on large samples (30 mm/5-8 mm initial diameter/height) and do not consider the microscale localised heterogeneities in the tissue. In those experiments, they do not differentiate between GM and WM and more importantly they did not take into account the anisotropy of brain tissue because of the directionality of axons in WM. Moreover, their perfusion based experimental set up is not compatible with the CED which instead requires infusion-based approach. Furthermore, they do not investigate the effect of time post-mortem on hydraulic permeability; there are not information about only GM or only WM, neither clarifications about the effect of the directionality in WM. Therefore, in order to obtain the hydraulic permeability which can be used for the applications like intratumoural infusions in CNS, localised measurements on WM with a precise infusion-based experiments are needed. Additionally, the anisotropy in WM due to the directionality of axons in the matrix [Pieri et al.,

2019][Winklewski et al., 2018][Walhovd et al., 2014] makes its hydraulic permeability direction dependent. So far not much attention has been paid to this and only a few theoretical studies have reported the effect of anisotropy of brain WM on the hydraulic permeability [Zhan et al., 2019]. To the best of authors' knowledge no experimental study has considered the anisotropy of WM at the localised scale and has investigated the effect of directionality of axons on its hydraulic permeability.

For these reasons, in this study the permeability of only WM, from directly measured parameters, was calculated, investigating the effect of anisotropy of WM and exploring the changing of permeability with post-mortem time. A large diameter reservoir and commercially available thermal flow sensor were used. Specifically, the flow rate was calculated based on thermal gradient along a capillary tube, induced by a small heating element. Knowledge of the applied pressure, the resistance of the flow sensor and the flow rate through the sensors provided redundant information, used to monitor the functioning of the flow sensor itself (for example, to detect blockages).

Chapter 3

MATERIALS AND METHODS

In this chapter, the materials and the methods to run the experiments are presented. In Sec. 3.1, the brain tissue and the tools used are described. In Sec. 3.2 the way how the samples are harvested is in depth illustrated. In Sec. 3.3, the set up used for the experiments is presented while in Sec. 3.4 the experimental protocol is analysed. The data analysis with the statistical details and the the statistical analysis of the permeability data are presented respectively in Sec. 3.5 and Sec. 3.6. Moreover, the Sec.3.7 describes the numerical analysis, parallely conducted to the experimental one, with the solver ANSYS.

Fig. 3.1 schematically shows how the authors conducted this study. From the experimental point of view, all the steps conducted on the preparation of the brain tissue and of the apparatus represent the preliminary phase. Consequently, the perfusion was performed on both samples with parallel and perpendicular fibres to the direction of the needle. Finally, after the filtration of the data, the calculation of the hydraulic permeability, k, with Darcy's law (Eq. 2.1) has been done. In this phase, the authors were moved by the question of which measure of thickness of the sample was the correct one. More clearly, as the infusions provided a needle inserted for half thickness of the specimens, the doubt was if using in the equation the thickness of the sample under the needle or the total thickness. So, for this reason, fluid dynamic simulations, the most similar to the reality, were performed, according to the experimental data obtained from the experiments. The analysis of the velocity paths of the particles inside the

samples during the perfusions, demonstrates that the total thickness of the samples is involved.

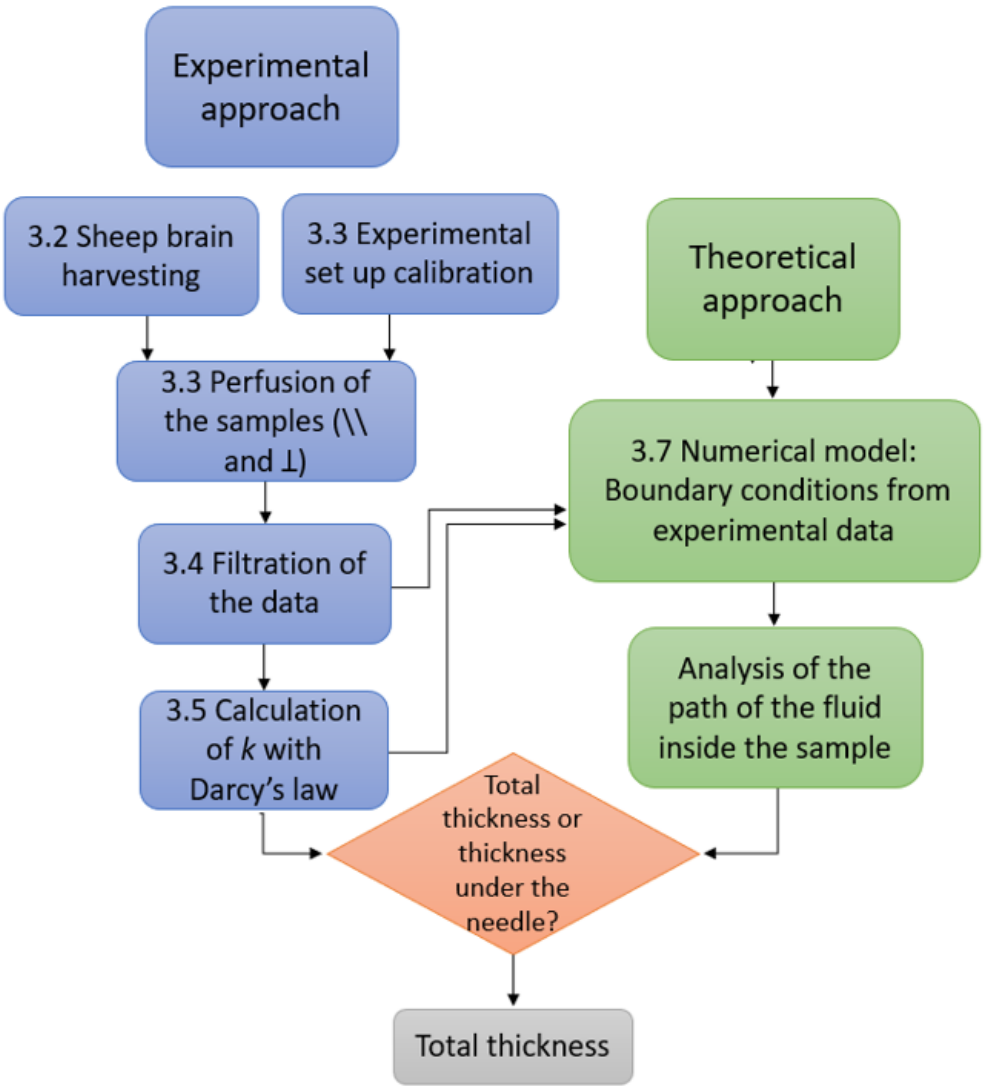

Figure 3.1: *Workflow of the study conducted in this thesis. An experimental approach was faced in parallel to a theoretical one, using the experimental results.*

3.1 Materials

Ovine brains were obtained from a local slaughterhouse as by-products of the commercial slaughter process. Brains were extracted from the heads of sheep by carefully opening the skull and avoiding any damage to the brain, within 1 hour post-mortem at the slaughterhouse. Immediately the brains were placed in a cylindrical glass container

and transported to the laboratory for further sectioning and performing experiments. During the sample preparation and performing experiments, phosphate-buffered saline (PBS), pH 7.4, and a concentration of $1X$ (PBS already diluted with the same concentration of deionised water), at room temperature was used to store the brain at room temperature. Animal brain tissue is widely used as a substitute for human brain tissue because of the high degree of similarity in terms of anatomical structures and mechanical properties [Nicolle et al., 2004].

3.2 Sample preparation

The samples were harvested from the brain following the same protocol, in order to obtain consistent samples. For each hemisphere, sagittal and coronal cuts were performed, obtaining slices 7-8 mm thick (Fig. 3.2). This procedure allowed seeing the WM regions from each slice. In this study, it is focused especially on corona radiata (CR) because it is a region where it is possible to collect WM samples of such dimensions. Initially, also samples from corpus callosum and fornix were harvested, but thew were not sufficiently thick to be tested.

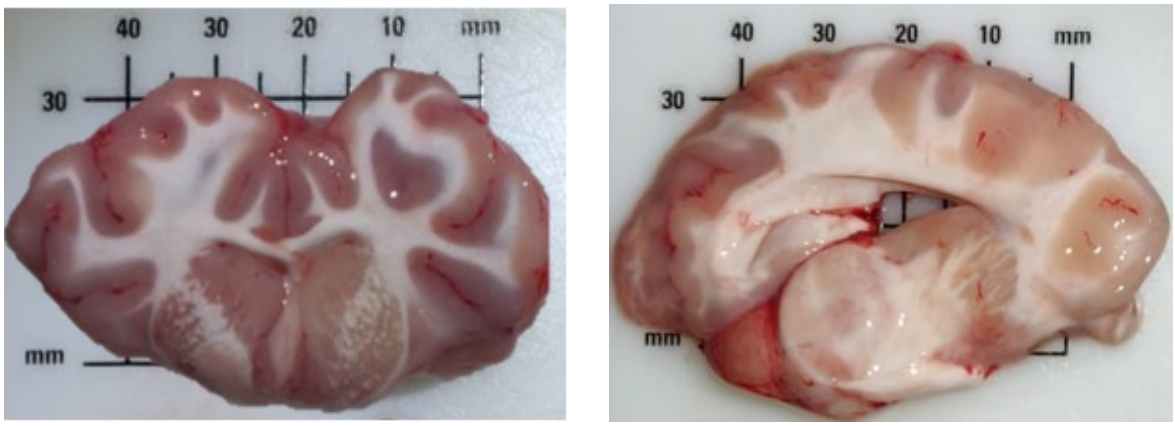

Figure 3.2: *(a) Coronal ovine brain slice. The radiation of the corona radiata is well visible and also the corpus callosum, which connects the two hemispheres, is well recognizable. (b) Sagittal ovine brain slice. From this view part of the corona radiata and the fornix constitute the WM visible.*

The reason why both cuts were used is related to the fact that samples with perpendicular and parallel fibres were tested. Cylindrical samples (5 mm diameter) were

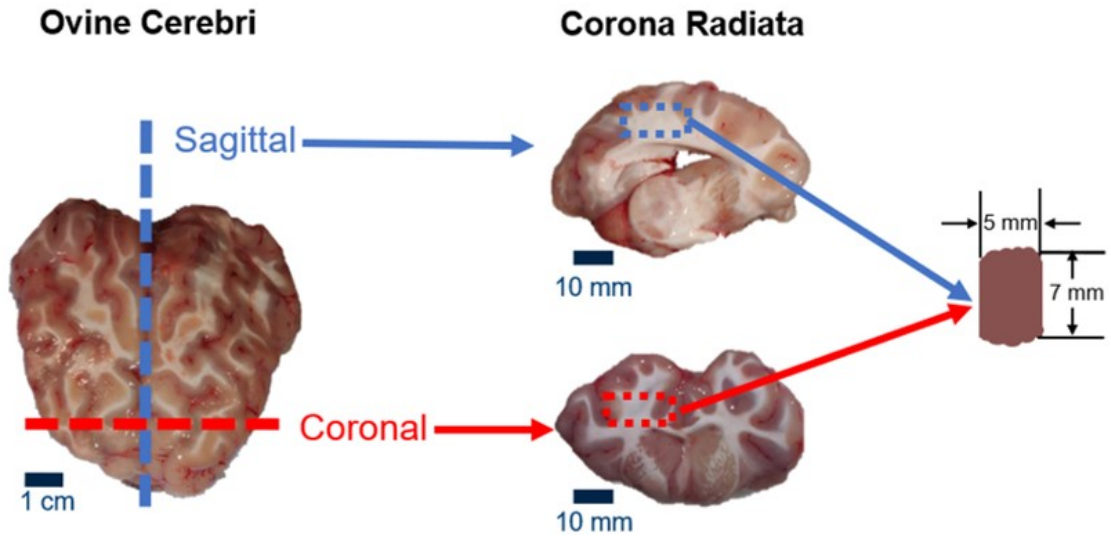

Figure 3.3: *Representative picture of ovine brain and the coronal and the sagittal cut slices where the corona radiata, used for making the samples, is highlighted by dotted rectangle.*

obtained from sagittal or coronal cut slices using surgical scalpels and blades (Fig. 3.3). The direction of the fibres within each harvested zone is known from literature. The exact disposition is animal-specific, but the general trend is predictable (Fig. 3.4).

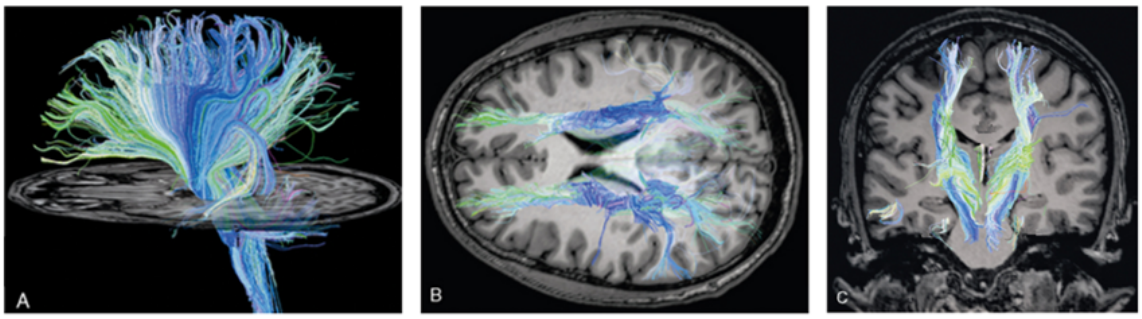

Figure 3.4: *Diffusion tensor tractography of the corona radiata. Sagittal image (A) shows the radiating projection of the fibres. A sample harvested from a perpendicular cut to this image presents perpendicular fibres to the direction of the tube. Axial image (B). Coronal image (C). Here the fibres are outgoing/incoming to the paper, so a sample harvested perpendicularly to this cut shows the fibre parallel to the direction of the tube. Picture modified courtesy of [Naidich et al., 2016].*

This preparation was performed on a sectioning board covered by superabsorbent paper kept wet by frequent spraying PBS thus avoiding dehydration of the tissue. Meanwhile,

samples holders were prepared by removing the tips of disposable transparent plastic pipettes to have only the cylindrical central part. At this point, a sized specimen was slowly 'sucked' in the pipette, trying to avoid deformations of the tissue. The specimen dimensions were consistent with the one of the plastic tube and perfectly fitted in its 'holder', the plastic tube 7 mm in length (Fig. 3.5). The resultant brain samples, 5 mm in diameter and 7 mm in height, inserted in plastic tubes, were divided into samples with axons parallel ($S_{\parallel}$) and axons perpendicular ($S_{\perp}$) to the long axis of the tube. They were stored in a petri dish with PBS, ensuring the hydration of the tissue. According to the health and safety guidelines of the Imperial College London, the brain waste was first collected in biohazard bag placed in small rigid boxes then stored stored in the freezer and eventually was properly disposed.

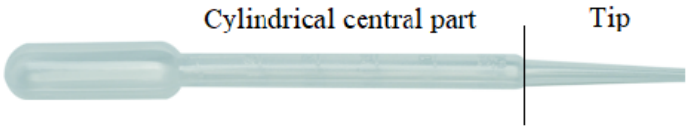

Figure 3.5: *Pipette used as 'holder' of the samples. The tip was removed, in order to have a plastic tube with a constant diameter (5 mm).*

3.3 Experimental set-up

The experimental apparatus is shown in Fig. 3.6. This set-up, named *iPerfusion*, comprises hardware and control software. It was initially developed for the measurement of outflow facility by ocular perfusion because it is extremely sensitive to small errors and all the techniques present in the literature have not been sufficiently validated and have considerable limitations [Sherwood et al., 2016]. The hardware consists of an actuated reservoir, a thermal flow sensor (SLG64-0075; Sensirion AG, Switzerland), and a differential pressure transducer (PX409; Omegadyne, USA). The pressure applied to the system is controlled using a 10 ml reservoir, filled with water. The height of the pressure reservoir is controlled using a linear actuator that has a stepper-motor with a micro step size of 1.25 μm which corresponds to a pressure change of 0.00009 $mmHg$.

The fluid passes from the actuated reservoir through the flow sensor, which comprises a 75 μm diameter glass capillary. Based on the knowledge of the flow characteristics (Poiseuille), the flow rate can be calculated in the range 5000 to 5000 nl/min, with an accuracy of 10% of the measured value. The pressure difference across the outflow pathway is measured using a silicon micromachined wet-wet differential pressure transducer. It has a range of 0−50 $mmHg$, and an accuracy reported by the manufacturer of 0.08% of the full-scale range, corresponding to 0.04 $mmHg$. On either side of the pressure transducer, a manifold is used to control the flow path, in order to switch between configurations required for sensor calibration and system validation. The brain samples were inserted in a glass bath, positioned on plastic support which presents four holes. The specimens with their tubes were inserted in the holes, guaranteeing a space between the bottom part of the tissue and the base of the bath. They are completely submerged in PBS, at room temperature (Fig. 3.7). Submersion ensures the hydration of the tissue during all the duration of the experiment. Moreover, thanks to the strategic position of the bath, downstream the flow sensor, the pressure transducer directly measures $P(t)$, the pressure inside the tissue, already adjusted of the pressure drop due to the small diameter capillary of the flow sensor $\Delta P_{\mathrm{q}} = Q(t)/C_{\mathrm{q}}$. On the contrary, the submersion depth, h_{b}, has no effect on the pressure drop across the outflow pathway. In fact, in the calculation of $P(t)$, it appears twice, simplifying itself. $\rho g(h_{\mathrm{r}} + h_{\mathrm{b}})$ is the positive contribution, always present into the brain sample, also with zero flow rate, and so it is the pressure created due to the height of the reservoir with respect to the surface of the fluid in the bath, $h_{\mathrm{r}}, (\rho g h_{\mathrm{r}} = P_{\mathrm{a}})$, and the part of the fluid on the samples, properly h_{b}. But the last one, $\rho g h_{\mathrm{b}}$, represents the hydrostatic pressure, and so the negative contribution on $P(t)$:

$$P(t) = \rho g(h_{\mathrm{r}} + h_{\mathrm{b}}) - \rho g h_{\mathrm{b}} - \Delta P_{\mathrm{q}} = P_{\mathrm{a}} - Q(t)/C_{\mathrm{q}} \tag{3.1}$$

For this study, two duplicates of the experimental setup were used, so two specimens could be measured simultaneously.

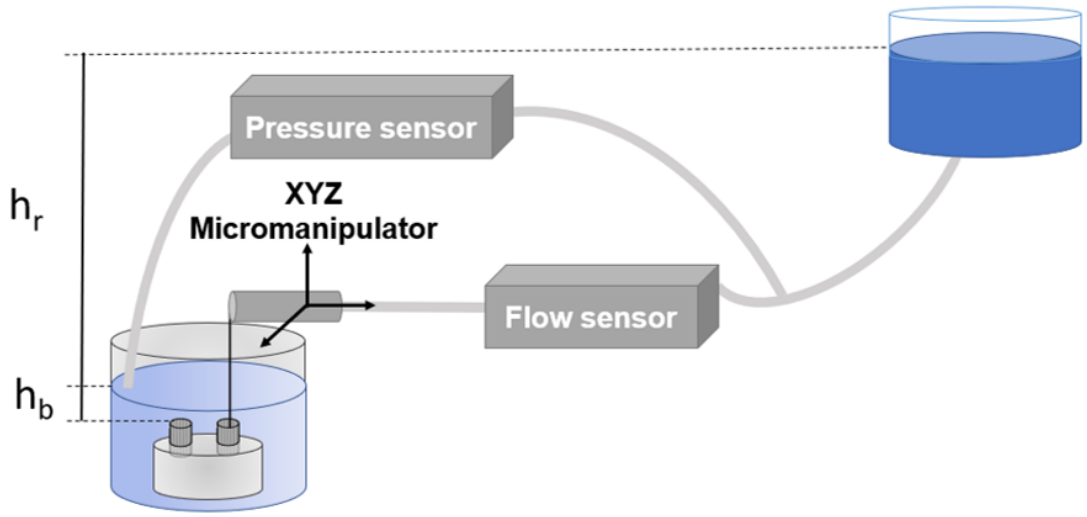

Figure 3.6: *Experimental set-up redrawn after inspiration from [Sherwood et al., 2016]. The inlet reservoir, the pressure and the flow sensors, the bath where the specimens are placed and the micromanipulator, to insert the needle in the samples for a known thickness, are the principal components of the apparatus.*

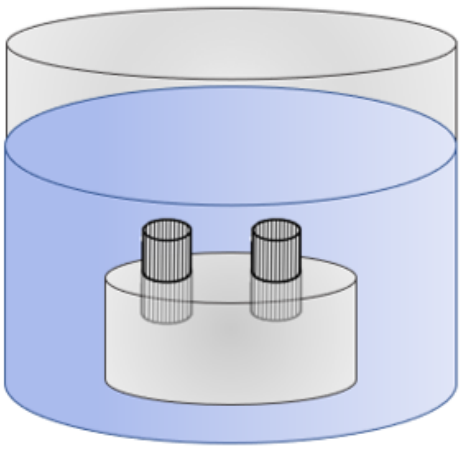

Figure 3.7: *Glass bath with two samples inserted in their 'holders', placed in the plastic support, completely immersed in the PBS. This arrangement ensured a space between the bottom part of the samples and the base of the bath, avoiding an occlusion on the inferior outlet.*

3.3.1 Experimental set-up calibration

The pressure sensor was calibrated each day of experiments. Firstly, the pressure on both sides of the sensor is set to be exactly equal, corresponding to zero pressure difference, recording the voltage output from the pressure sensor. The control software programmatically locates the height that gives the voltage recorded in the first step, which by definition corresponds to zero pressure. An eight-step automated calibration is then carried out, increasing P_{a} in increments of 60 mm, and averaging the voltage over 5 seconds at 1000 Hz for each step (in order to minimise the influence of electrical noise). Successively, the resistance of the flow sensor was measured to ensure that it was blockage free. Finally, before starting perfusion, the resistance of a glass capillary of known resistance was measured to confirm that the system was functioning properly. The perfusion tubing (downstream of the flow sensor) and needle (BD Microlance Stainless Steel Needles; 30G x ½"; $0,3$ x 13 mm) were then filled with PBS and the resistance of the needle was measured. As the fluid in the system was water, there was a water-PBS interface in the perfusion tubing. However, given that the volume of the tubing (about 2 ml) was large compared to the total volume perfused in an experiment (about 25 μl), neither advection nor diffusion could have altered the PBS entering the brain. If any of the readings from the tests were unexpected, for example, if the system time-response was too long or measured resistances were not correct, leaks/bubbles/blockages were identified and removed before the perfusion commenced. The insertion depth of the needle, always of 3 mm, was controlled by the moving arm of a graded micromanipulator (World Precision Instruments, USA).

3.4 Experimental protocol

The applied pressure was held at 7 $mmHg$ for a period of 25-30 minutes to allow the brain sample to acclimatise to the pressure environment. After acclimatisation, an eight-step perfusion protocol was carried out, consisting of applied pressures of $10, 12.5, 15, 17.5, 20, 22.5$ and 25 $mmHg$.

After the steady state has been reached, the step increases automatically. The parameter $\Gamma(t) = Q(t)/P(t)$ was continuously evaluated and $d\Gamma/dt$ was estimated by

linear regression over a moving window of 5 minutes. When $|d\Gamma/dt|$ was continuously less than 5 $nl/min/mmHg/min$ for one minute, the system was considered to be at steady state. The measured flow and pressure were then averaged over the four previous minutes to yield Q_{j} and P_{j} respectively, for pressure step j_{th}. The first pressure step used in the present protocol has been selected to be around the normal cerebral spinal fluid (CSF) pressure in ventricles (7 $mmHg$), equivalent to 10 cm column of CSF [Milhorat, 1972]. Both the range and the number of pressure steps are arbitrary and can be tailored to a particular experiment but should be held constant as much as possible for comparing cases within a given experiment. The duration of each experiment was 2 hours. However, in certain occasion a specimen could suffer abrupt disruption due to the big flow rate across the tissue or some imperfections inside the sample. At the end of the perfusion, the software returns some measurements for each pressure step of the protocol, such as instantaneous flow rate into the tissue and its standard deviation (nl/min), instantaneous pressure drop across the outflow pathway and its standard deviation ($mmHg$), applied pressure drop across the system, equal to $\rho g h_{\mathrm{r}}$ ($mmHg$), total outflow facility ($nl/min/mmHg$). The data file includes the row data and also the filtered ones, averaging of the last 4 minutes of the steady state period.

Firstly, the steps must be located in the acquired data: in fact after that the signal is selected, a smoothing filter is applied (all the data are filtered in the same way to be coherent and to compare the data) and finally the code calculates the derivative of the signal, identifying the peaks. Note that a stronger filter smooth the data more effectively, but also trims the data, reducing the sample size.

3.5 Data analysis

The parameters involved in this calculation were: the resulting pressure drop $P(t)$ on the sample due to the applied pressure P_{a}, the flow rate $Q(t)$ across the sample, the viscosity, μ, of the fluid (PBS) used for the perfusions, the area, A, and the thickness, L, of the sample through which the fluid flows. The first two measurements, $P(t)$ and $Q(t)$ are available from the system, μ was obtained from the chart of the fluid, available online and A, L are related to the characteristics of the geometry of the brain

sample. In this way, it was possible to calculate the intrinsic permeability k with Darcy's law (Eq.2.1), that describes the flow of a fluid through a porous medium. The complete dataset comprises 71 brain samples, of which 44 with parallel fibres and 27 with perpendicular ones. Specifically, the weighted averages were calculated on 306 total valid pressure steps, of which only 167 are the steps of experiments with samples with parallel fibres. In fact, these last samples were subjected to big flow rates that, often, caused the disruption of the specimens with the highest pressure steps. The brain samples, all harvested from Corona Radiata, present different ages post-mortem, from 3 hours to 1 day.

It is not clear whether differences in post-mortem times cause variation in the mechanical response of the tissue; while some researchers show no [Budday et al., 2015] [Darvish and Crandall, 2001] [McElhaney et al., 1973] or limited [Nicolle et al., 2005] [Shen et al., 2006] changes in the measured properties due to different post-mortem times, [Metz et al., 1970] reported changes from live to 45 min post-mortem times and [Garo et al., 2007] showed an increase in the stiffness in the first 6 h post-mortem. According to this last study, the data are divided into different groups, considering before and after 6 h post-mortem.

3.6 Statistical analysis

Lilliefors test was used to verify if data samples came from a normal distribution (null hypothesis). The test was performed on Matlab, considering four independent groups, Parallel$\leq$6 h, Parallel>6 h, Perpendicular$\leq$6 h, Perpendicular>6 h. Only the first group resulted a normal distribution, with a p-value of 0.1983. The others distribution were not normal with a p-value of 0.001, 0.001, 0.0016 respectively. As explained in Sec.1.4 the localised hydraulic permeability of the four groups has been investigated in order to identify statistical differences. So, to test if the permeabilities come from distributions with equal medians (null hypothesis, H_0), the non parametric Jonckheere-Terpstra statistical test was used to asses. Specifically, the Jonckheere-Terpstra test is a rank-based non parametric test that can be used to determine if there is a statistically significant trend between an ordinal independent variable and a continuous or ordinal

dependent variable.
Six assumptions are required in order to have a valid result (available at the website: https://statistics.laerd.com):

1. The dependent variable should be measured at the ordinal or continuous level ($\leq$6 h (3-6 hours); >6 h (7-12 hours));

2. The independent variable should consist of two or more ordinal, independent groups (two groups: parallel fibres; perpendicular fibres);

3. Indipendence of observations, it means that there is no relationship between the observations in each group or between the group themselves;

4. It is needed that the distributions in each group (i.e., the distribution of scores for each group of the independent variable) have the same shape and the same variability. This allows to use the Jonckheere-Terpstra test as a test of medians;

5. It is needed to predict, a priori, the order of the groups of the independent variable when running the Jonckheere-Terpstra test (i.e., the term, "a priori", simply means that you have to predict this order "before" you collect your data, typically when you set the research questions/hypotheses for your study);

6. It is needed to predict, a priori, the direction of the alternative hypothesis. This assumption ensures that this is a prediction and not based on you having been able to evaluate the data first.

For both cases, H_0 was rejected and so, the alternate hypothesis, H_1, was accepted. It means that the medians of the groups are related by a relationship as follows: $Mdn_1 \leq Mdn_2 \leq ... \leq Mdn_{\mathrm{k}}$, where at least one of these $\leq$ can be replaced by $<$.

3.7 Hydraulic permeability simulations

3.7.1 Introduction

In this study, the hydraulic permeability of the brain was calculated with Darcy's law (Eq.2.1). Since a different approach with respect to the classical conditions of application of the equation was used, a parallel numerical study was necessary. As the authors showed in Sec.3.3.1, the flow passing through the specimen was injected from a needle, inserted for half thickness of the specimen, with the possibility to exit from the upper or lower part of the sample. Therefore, it was necessary to understand if the flux was mainly directed to one outlet or both, thus considering a specimen thickness of 3.5 mm or 7 mm respectively.

3.7.2 Numerical model

The geometry implemented reproduces the real one in a 2-D domain for symmetry reasons. The needle was modeled cropping the area of the needle (3 x 0.0795 mm) from the one of the samples (Fig. 3.8). Moreover, to include also the walls of the needle, a rectangular region, 3 x 0.0762 mm, was defined as a solid region. Simulations on this bi-dimensional geometry were run applying an axisymmetrical condition. The boundary condition at the inlet (mass-flow-inlet) was chosen according to the experimental flow rate, measured during the infusion; the correspondent velocity indicates a very low Reynold's number ($Re \approx 10^{-5}$) respecting Darcy's law hypothesis. Specifically, the mass-flow-inlet was imposed equal to $2.34 \cdot 10^{-10}$ kg/s to simulate the sample with parallel fibres and equal to $1.48 \cdot 10^{-10}$ kg/s for the sample with perpendicular ones. A zero-pressure was applied at the open surface on the upper part of the sample (outlet_up), and a pressure equal to 68 Pa ($P = \rho g h$, where ρ is the fluid density, g is the gravity acceleration, h is the thickness of the specimen), trying to reproduce the condition of the samples in the bath, completely immersed in the fluid. A no-slip condition was set on each wall. The specimen was modeled as an anisotropic porous media imposing two permeability values, average of the experimental data ($9.17 \cdot 10^{-16}$ m^2, $9.17 \cdot 10^{-17}$ m^2). The higher and lower permability values were imposed on the

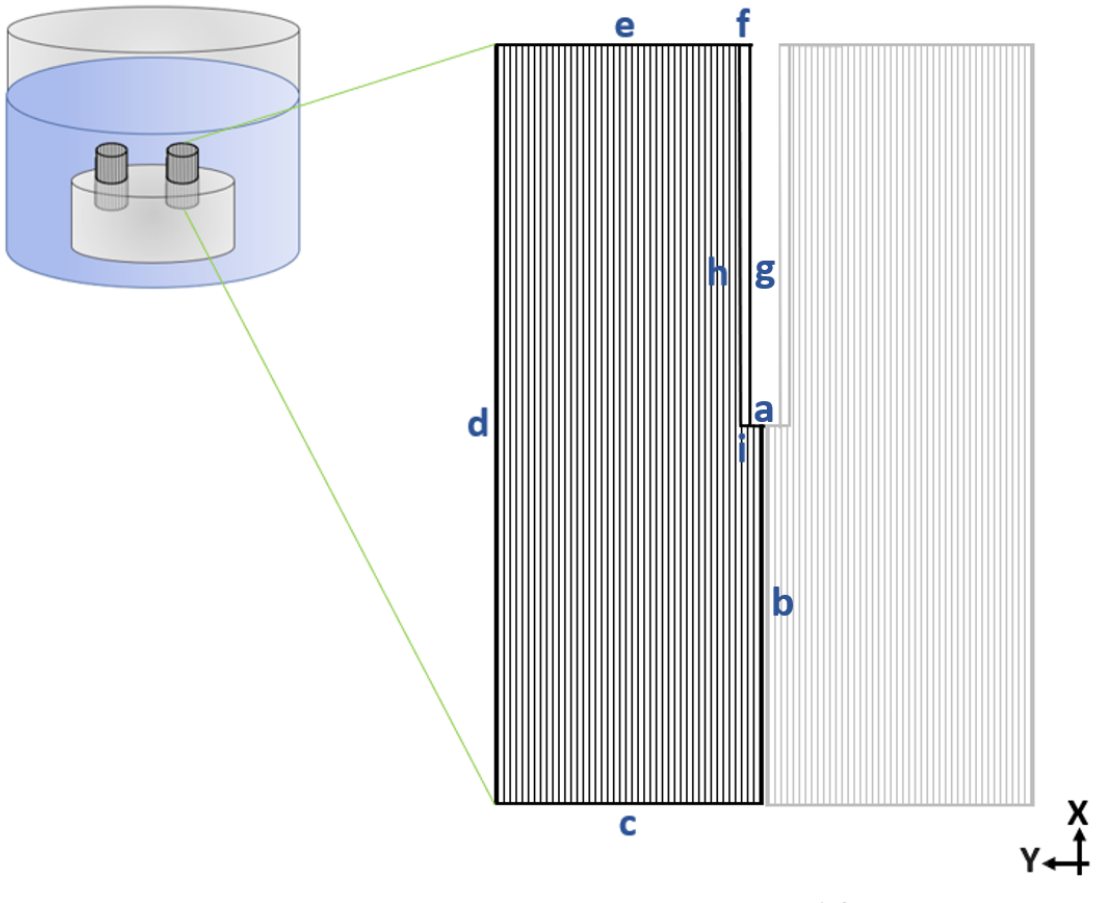

Figure 3.8: *Geometry in the plane X-Y.* ***a*** *corresponds to the inlet,* ***b*** *represents the axys,* ***c*** *and* ***e*** *are the outlet_down and the outlet_up, respectively. Moreover* ***d***, ***f***, ***g***, ***h*** *and* ***i*** *correspond to the walls. The rectangular defined by the edges* ***f***, ***g***, ***h***, ***i***, *is the surface that simulate the wall thickness of the needle; the empty space defined by the edges* ***a*** *and* ***g***, *is the surface that simulate the internal diameter of the needle. In the simulations only half of the geometry was implemented, the semi-transparent geometry indicates the symmetric portion.*

needle direction in the $S_{\parallel}$ and $S_{\perp}$, respectively.

The solution was computed solving the Navier-Stokes equation by means of the finite element method (FEM) solver ANSYS (ANSYS, Lebanon, NH) with semi-implicit methods for pressure linked equations (SIMPLE) [ANSYS, 2017].

Chapter 4

RESULTS AND DISCUSSION

In this chapter the results of the experiments will be presented. Each section shows the analysis of the data considering different parameters. The effect of directionality of axons on the flow across the tissue is described in the Sec. 4.1 whereas the Sec. 4.2 faces the effect of pressure on flow rate and permeability. Finally, the Sec. 4.3 describes the effect of post-mortem time on the hydraulic permeability.

4.1 Effect of directionality of axons on the flow across the tissue

Fig.4.1 (a) and Fig.4.2 (a) show the representative flow rate and pressure traces with respect to time during the infusion experiments on WM tissue samples, $S_{\parallel}$ and $S_{\perp}$, respectively, both harvested within the 6 h post-mortem time. For every discrete pressure step, the flow rate immediately rises to a peak value because of the sudden increase in pressure but then quickly drops by about 80% of the peak value in the first minute and then continue to drop slowly. During the eight steps infusion protocol, the pressure at each step is held constant until the tissue adjusts itself to the new pressure environment, so reaching the steady state condition (Sec. 3.4). For $S_{\parallel}$, the flow rate rises with increasing applied pressure from about 128 nl/min at 7 $mmHg$ to about 558 nl/min at 25 $mmHg$. However, for the same set of applied pressure

steps, the flow rate across $S_\perp$ is much lower and rises from about 7 nl/min at 7 $mmHg$ to about 27 nl/min at 25 $mmHg$. Both samples have similar profiles of flow rates but different quantitatively. Flow rate across $S_\parallel$ can reach as much as 20 times higher than the flow rate across $S_\perp$. This is due to the fact that the flow across the tissue is strongly dependent on the porous media structure which offers a very different resistance depending on the flow direction. Indeed, WM is composed of aligned myelinated axons (axon diameter ranges 0.1-10 μm) and relatively soft extra cellular matrix (ECM) [Alexander et al., 2019]. When the axons are parallel to the direction of the flow, a consistent number of axons is directly interested from the flow exiting from the tip of the needle, collecting and directing the flow to two "outlets", the bottom and the upper cross-sections (the lateral area of the specimen is, in fact, bounded by the plastic holder). On the contrary, with axons perpendicular to the direction of the needle, the flow must face a much more tortuos path [Vidotto et al., 2018] to go out from the specimen, that lead to a sharp decrease of hydraulic permeability. The cross-sections of the WM invested by the flow rate are shown in Fig. 4.1 (b) and in Fig. 4.2 (b).

These results demonstrate that directionality of axons in the tissue should be considered in investigating the infusion and permeability.

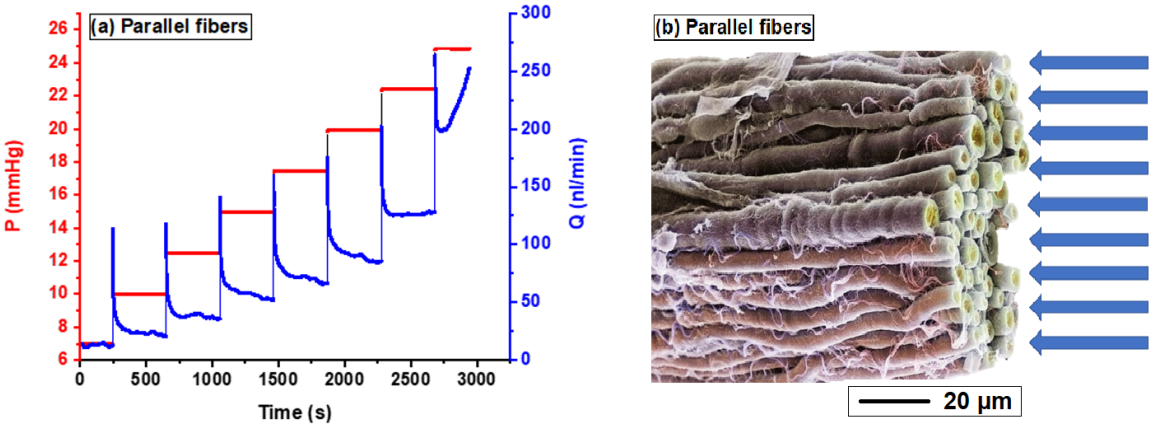

Figure 4.1: *(a) Flow rate and pressure traces with respect to time during the infusion in WM samples ($S_\parallel$). (b) Representative cross-sectional area of the sample with parallel fibre, at microscale. Picture adapted from: https://www.sciencephoto.com/media/307360/view/nerve-fibre-sem*

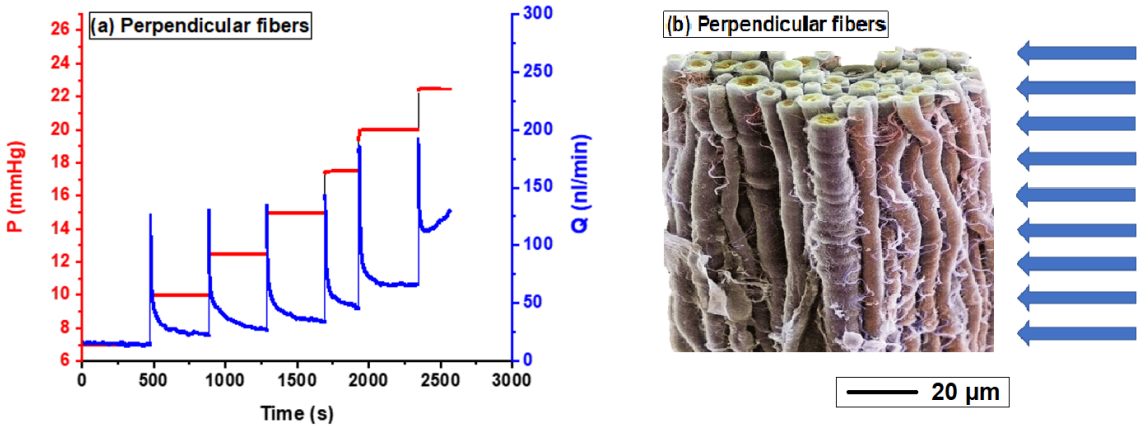

Figure 4.2: *(a) Flow rate and pressure traces with respect to time during the infusion in WM samples ($S_\perp$). (b) Representative cross-sectional area of the sample with perpendicular fibre, at microscale. Picture adapted from: https://www.sciencephoto.com/media/307360/view/nerve-fibre-sem*

4.2 Effect of pressure on the flow rate and permeability

A series of experiments were performed on samples $S_\parallel$ and $S_\perp$ harvested from different brains at different applied pressures to explore the flow behaviour across the tissue and its dependence on the directionality of axons in the tissue. In each experiment, please note that the actual pressure inside the tissue is slightly less than the applied pressure, because of the hydrodynamic resistance of the flow sensor (Sec. 3.3). Fig. 4.3 shows the flow rates across $S_\parallel$ samples ($Q_\parallel$) and across $S_\perp$ samples ($Q_\perp$) in response to increasing pressures inside the tissues. Taking into account that a localised measurement has been performed on a biological specimen, both inter-subject and intra-subject variability is expected and can be seen from the scatter in the data. Considering the mean values of flow rates, for $S_\parallel$ (Fig. 4.3 (a)), the flow rate has initially a large gradient and rises from about 60 to 158 nl/min as the pressure increases from 6.97 to 12.40 $mmHg$ and then reaches a relatively stable values about 190 nl/min at 22.38 $mmHg$. Note that, for a further increase in the applied pressure there is a sharp rise in the flow rate that reaches about 302 nl/min at 24.79 $mmHg$. In case of $S_\perp$ (Fig. 4.3 (b)), the same trend is visible but lower in magnitude. The flow rate first rises from about 16 nl/min to about 38.5 nl/min when pressure increases from 6.97 $mmHg$ to 17.48 $mmHg$ and

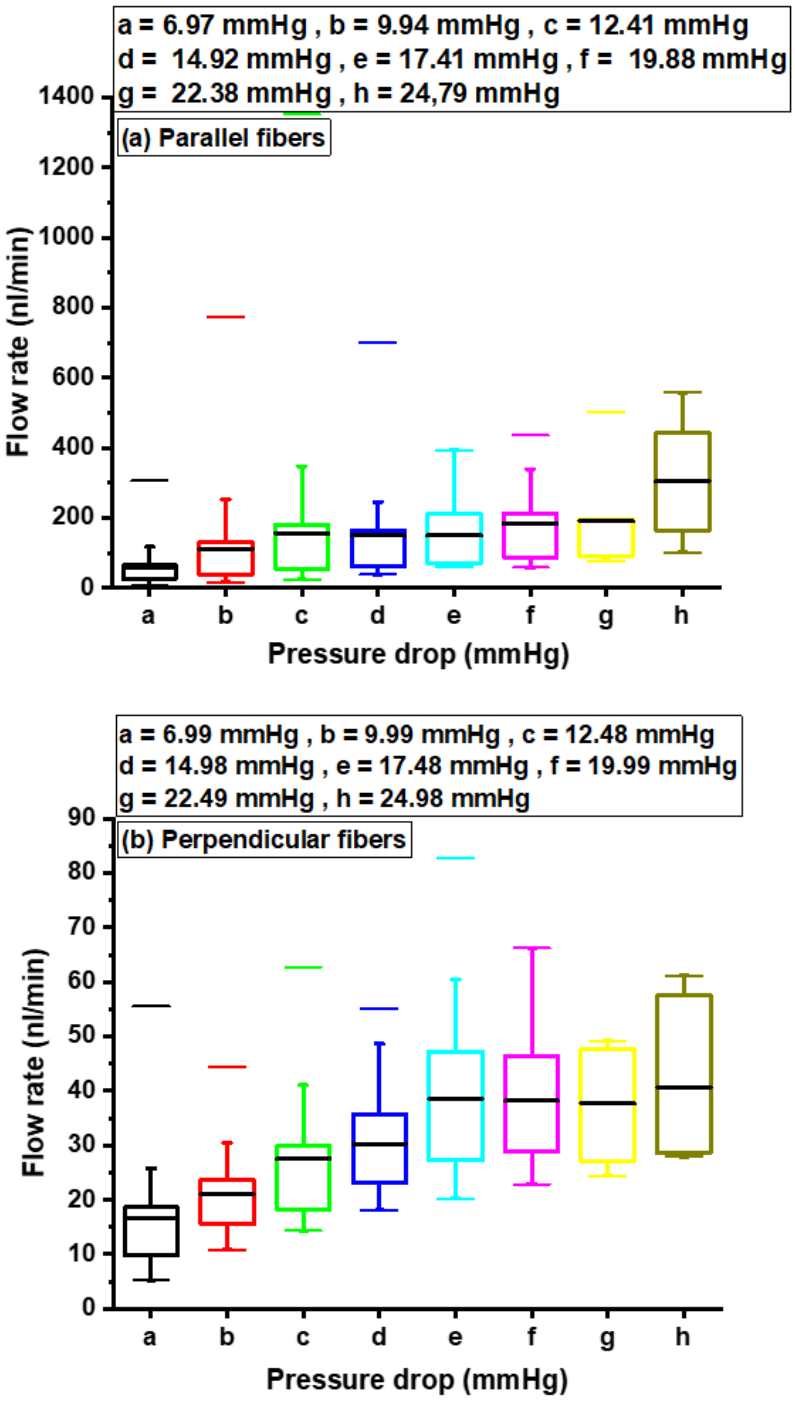

Figure 4.3: *Flow rate across the tissue (a) ($Q_{\parallel}$) and (b) ($Q_{\perp}$). The pressures (average values for each step) inside the tissue are slightly less than the applied pressure, because of the hydrodynamic resistance of the flow sensor.*

then relatively stabilises to a maximum value of about 40 nl/min at 24.98 $mmHg$.

A comparison of the flow rate across $S_{\parallel}$ and $S_{\perp}$ is shown in Fig. 4.4 and Fig 4.5,

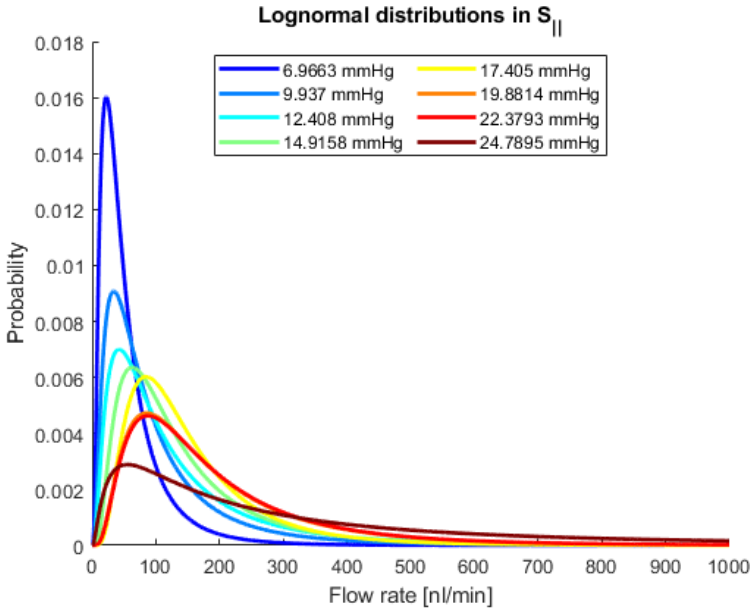

Figure 4.4: *Lognormal distribution of the flow rate across $S_{\parallel}$.*

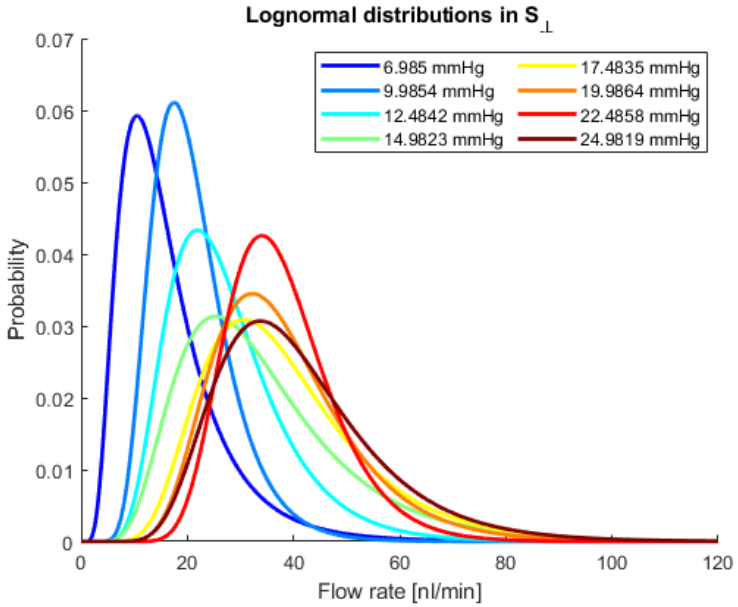

Figure 4.5: *Lognormal distribution of the flow rate across $S_{\perp}$.*

respectively. Both data sets, $S_{\parallel}$ and $S_{\perp}$ have similar lognormal distributions. The fact that $S_{\perp}$ is more converged than $S_{\parallel}$ because of its small values in comparison to $S_{\parallel}$, is visible from the two different scales of the X-axis. The ratio between the mean values of flow rates across $S_{\parallel}$ and $S_{\perp}$ ($\Delta Q = Q_{\parallel} \ / \ Q_{\perp}$) at the same pressures highlights the role of directionality of axons in understanding the infusion mechanism as shown in Fig. 4.6. The pressure threshold across $S_{\perp}$ is about 5 times higher than the one needed

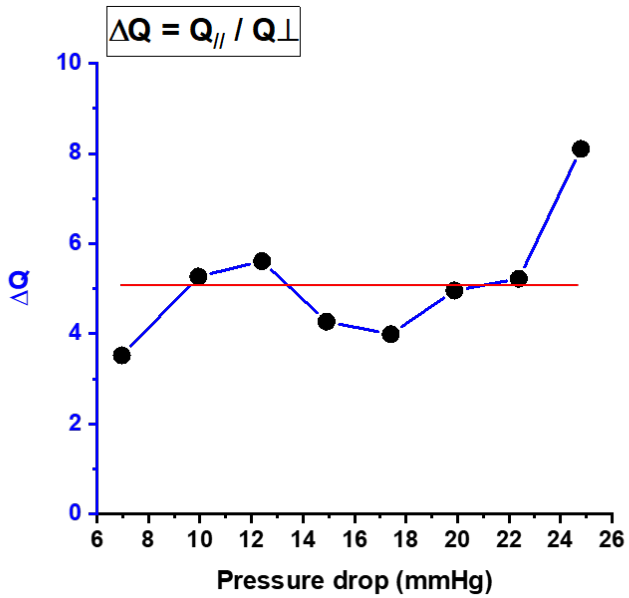

Figure 4.6: *The graph shows the ratio of the mean values of the flow rates against the pressure drop and the red line (5.11) is the average of the eight data points. It is possible to notice a constant value in ΔQ from 6.96 $mmHg$ to 22.48 $mmHg$ pressure, and a sharp rise at 24.79 $mmHg$ pressure related to a very large increase in $Q_{\parallel}$ with respect to $Q_{\perp}$ which remains the same. This suggests that at pressures of about 25 $mmHg$ or higher, the $S_{\parallel}$ microstructure starts to deteriorate while $S_{\perp}$ can sustain higher pressure.*

to infusate across $S_{\parallel}$. Furthermore, in Fig. 4.6, it is possible to notice a sharp rise in ΔQ at 24.79 $mmHg$ pressure due to a very large increase in $Q_{\parallel}$ with respect to $Q_{\perp}$ that remains the same. This suggests that at pressures of 25 $mmHg$ or higher, the $S_{\parallel}$ microstructure starts to deteriorate while $S_{\perp}$ can sustain higher pressure. It is harder to deform axons (stiffness of a single axon, $E = 9.5\ kPa$ [Ouyang et al., 2013]) than ECM (stiffness is a few hundred Pa [Wells, 2008]). In case of $S_{\parallel}$, the cross-sectional area of the tissue exposed to infusate pressure is composed of both, axons and the relatively soft ECM while in case of $S_{\perp}$, the exposed cross-sectional area is mostly composed of axons [Pieri et al., 2019]. Therefore, it is understandable if $S_{\parallel}$ deteriorates while $S_{\perp}$ can survive high pressures.

Fig. 4.7 shows the hydraulic permeability data of $S_{\parallel}$ and $S_{\perp}$. As expected, both $S_{\parallel}$ and $S_{\perp}$ have similar behaviour and the permeability does not change with increasing pressure and rather stays stable within the small fluctuations. However, quantitatively, there is significant difference between $S_{\parallel}$ and $S_{\perp}$. Comparison of Fig. 4.7 (a) and Fig.

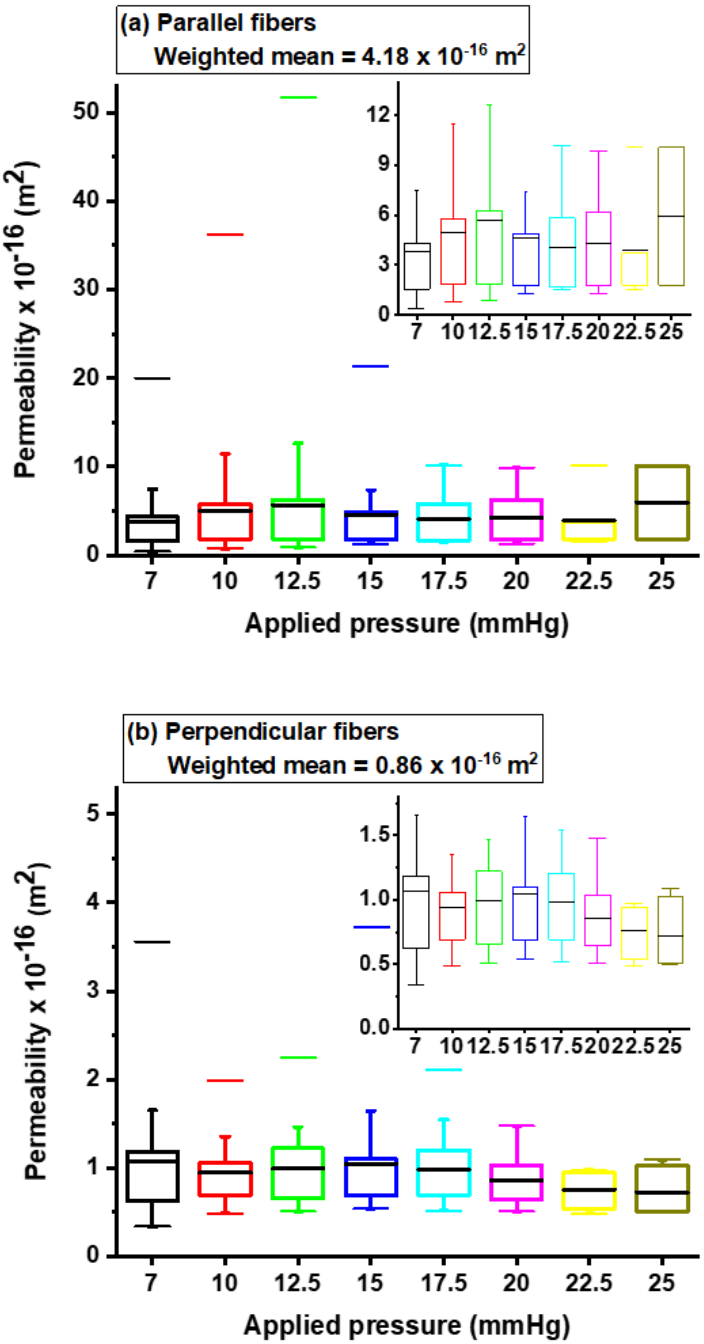

Figure 4.7: *Hydraulic permeability at different applied pressures across the brain white matter samples (a) $S_{\parallel}$ and (b) $S_{\perp}$. The insets show the corresponding zoomed data.*

4.7 (b) shows that the hydraulic permeability of $S_{\parallel}$ is about five times more than $S_{\perp}$. The weighted mean was calculated in order to take into account the number of samples for each pressure step, since not all the samples sustained the highest pressures. Eq.

4.1 shows the formula to compute the weighted permeability k where the weights (w_{i}) are the inverse of the squared standard deviation (σ) of each step (7, 10, 12.5, 15, 17.5, 20, 22.5, 25 $mmHg$), $w_{\mathrm{i}} = 1/\sigma^2$, that were standardised, $w_{\mathrm{st\ i}} = \frac{w_{\mathrm{i}}}{\sum_{j=1}^{m}} w_{\mathrm{j}}$, with j_{th} step of the same category ($S_{\parallel}$ or $S_{\perp}$):

$$k_{\mathrm{j}} = \sum_{i=1}^{n} \bar{P}_{\mathrm{i}} \cdot w_{\mathrm{st\ i}} \tag{4.1}$$

The weighted permeability for $S_{\parallel}$ is $4.18{\times}10^{-16}$ m^2 while that for $S_{\perp}$ is $0.86{\times}10^{-16}$ m^2.

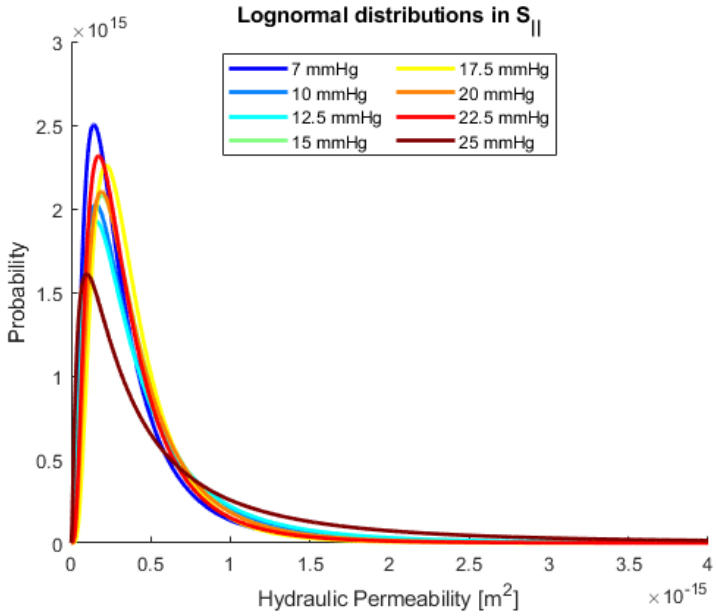

Figure 4.8: *Lognormal distribution of the hydraulic permeability at different applied pressure in $S_{\parallel}$.*

Fig. 4.8 and Fig. 4.9 show that both, $S_{\parallel}$ and $S_{\perp}$ samples have lognormal distributions. Also in this case the relatively converged distribution of $S_{\perp}$ can be seen from the different scales of X-axis. The analysis of the effect of pressure on the permeability was conducted also considering another parameter, the time post-mortem. It has been reported in literature that mechanical behaviour of brain tissue changes after 6 h post-mortem [Garo et al., 2007] and, it becomes stiffer. To explore it further, whether that will also change the hydraulic permeability, it has been investigated at post-mortem time $\leq$6 h and post-mortem time >6 h for both $S_{\parallel}$ and $S_{\perp}$ samples in response to different applied pressures. Fig. 4.10 and Fig. 4.11 show the hydraulic permeability at post-mortem time groups along with the representative pressure and flow rate traces with respect to time. The low p-value, 4.84 x 10^{-8}, resulting from the Jonckheere-

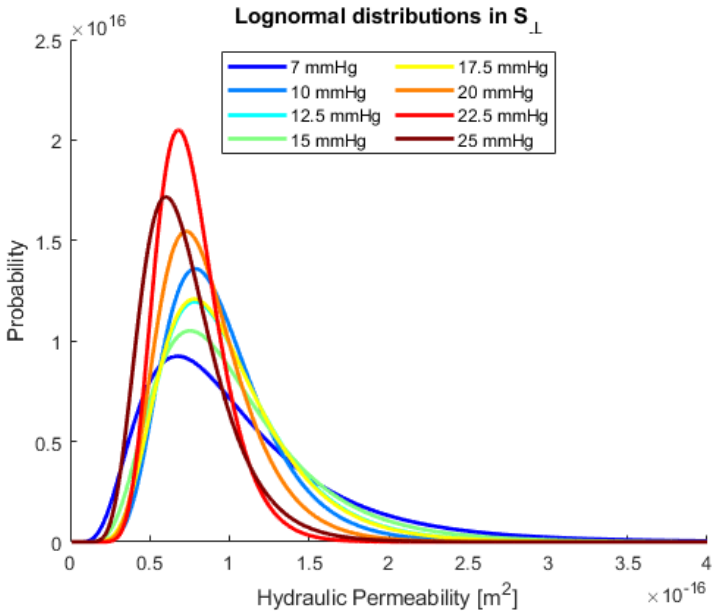

Figure 4.9: *Lognormal distribution of the hydraulic permeability at different applied pressure in $S_\perp$.*

Terpstra shows that there is a significant statistical difference between the median permeabilities of the four post-mortem time groups, $S_\parallel$ ≤6 h, $S_\parallel$ >6 h, $S_\perp$ ≤6 h, $S_\perp$ >6 h. For $S_\parallel$, the weighted mean hydraulic permeability is 4.03×10^{-16} m^2 and 4.48×10^{-16} m^2 at post-mortem time ≤6 h and >6 h, respectively. Similarly, for $S_\perp$, the weighted mean hydraulic permeability is 0.812×10^{-16} m^2 and 0.881×10^{-16} m^2 at post-mortem time ≤6 h and >6 h, respectively. So, from this test it can be inferred that there is a statistical difference between the hydraulic permeabilities of $S_\parallel$ and $S_\perp$ (Fig. 4.12). However, after performing this test, no information about which group is different from the others was obtained, because it reveals only if there is a difference. So, successively a post-hoc test was performed in order to examine the differences. Significance values have been adjusted by Bonferroni correction for multiple tests, which literally cuts off the significance level (α), becoming very rigorous. The final result is that there are statistical differences between:

- $S_\perp$ ≤6 h and $S_\parallel$ ≤6 h with a significance value of 0.0001;
- $S_\perp$ ≤6 h and $S_\parallel$ >6 h with a significance value of 0.0001;
- $S_\perp$ >6 h and $S_\parallel$ ≤6 h with a significance value of 0.0001;
- $S_\perp$ >6 h and $S_\parallel$ >6 h with a significance value of 0.001.

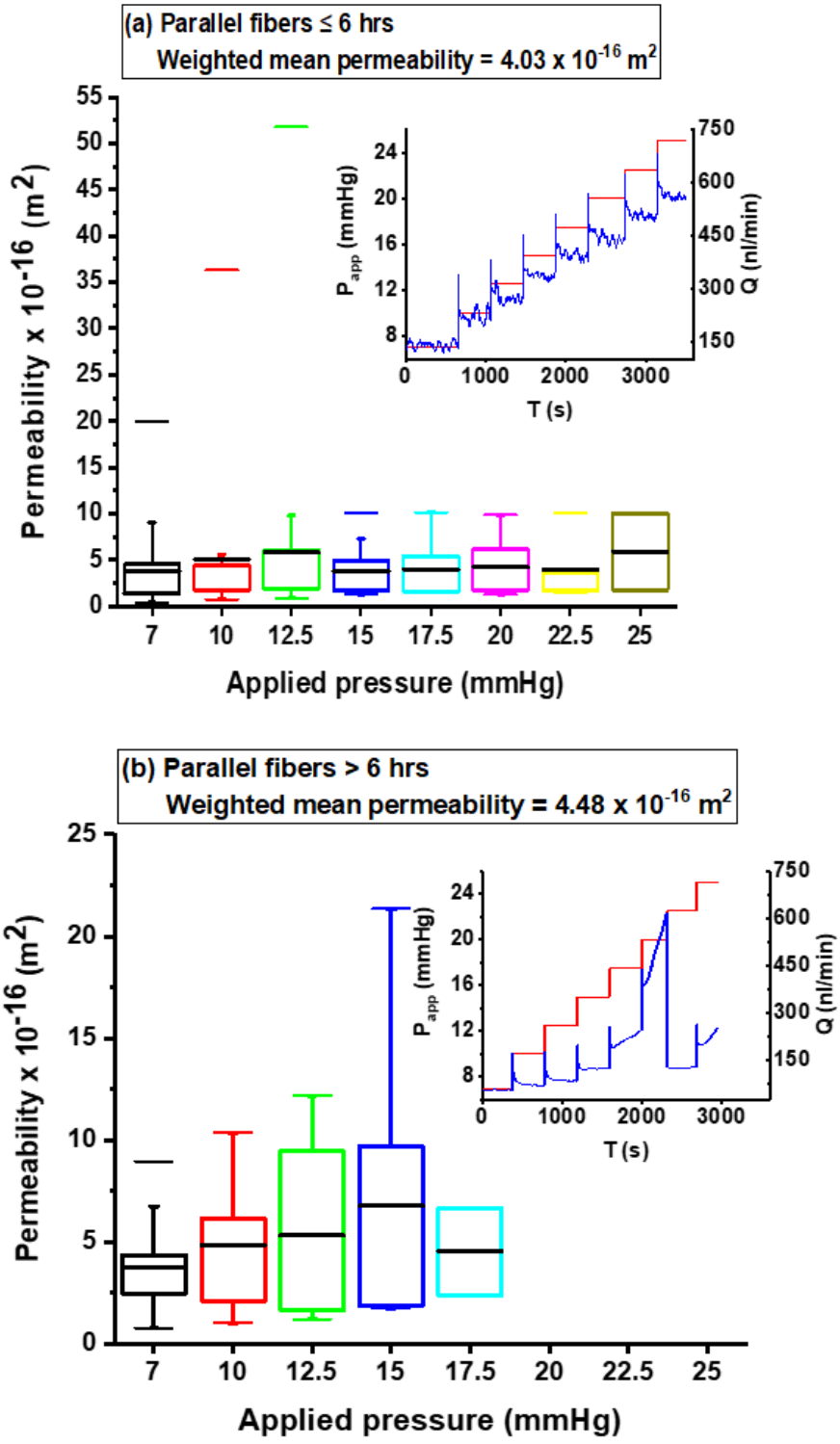

Figure 4.10: *Permeability of $S_{\parallel}$ at different pressures measured at post-mortem time (a) ≤6 h and (b) >6 h. Insets show the representative pressure vs flow rate traces with respect to time. From the (b) inset a drop in flow rate, at 22.5 mmHg, is visible, which means the rupture of the tissue.*

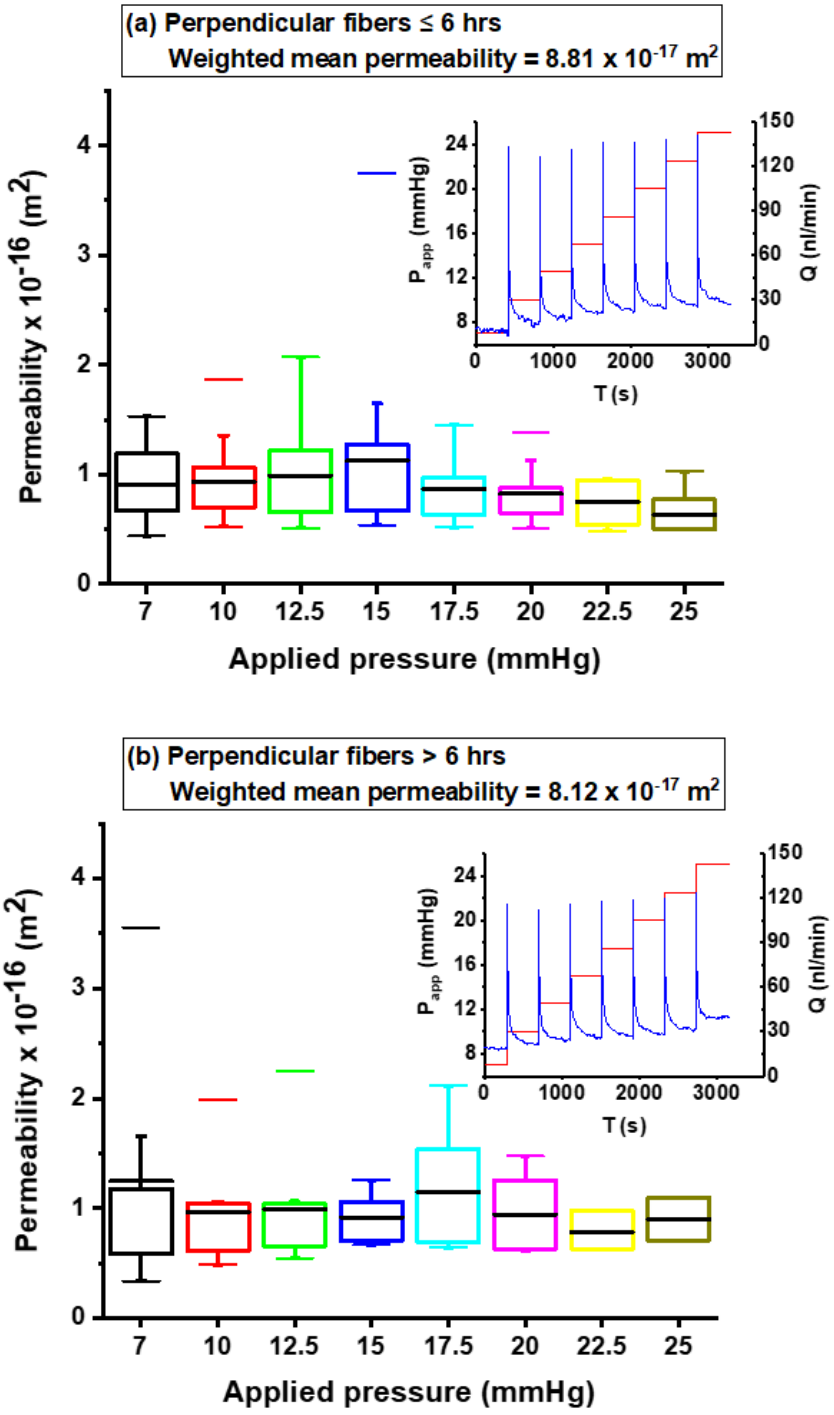

Figure 4.11: *Permeability of $S_{\perp}$ at different pressures measured at post-mortem time (a) ≤6 h and (b) >6 h. Insets show the representative pressure vs flow rate traces with respect to time.*

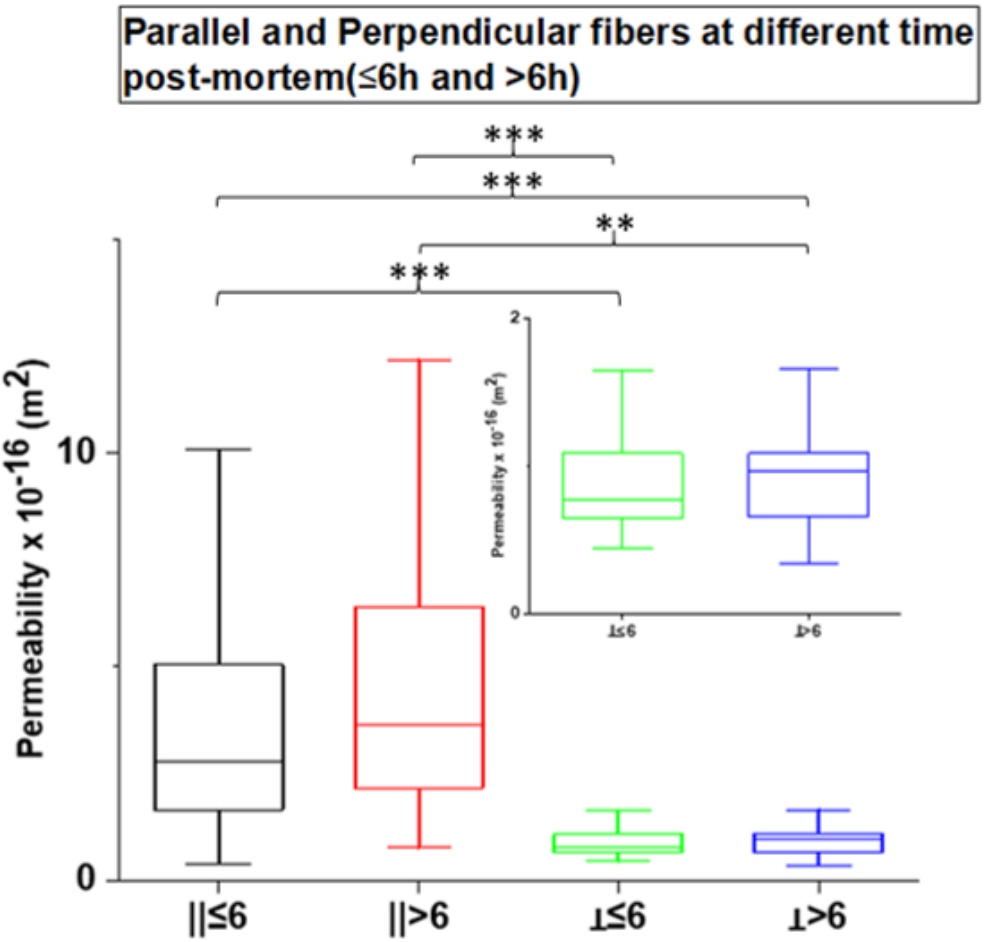

Figure 4.12: *Hydraulic permeability of the four statistical groups: $S_{\parallel}$ ≤6 h, $S_{\parallel}$ >6 h, $S_{\perp}$ ≤6 h, $S_{\perp}$>6 h. The inset shows the zoomed data of perpendicular fibres. From the graph emerges the statistical difference of pairwise comparisons after the Bonferroni correction. Specifically, between $S_{\perp}$ ≤6 h and $S_{\parallel}$ ≤6 h, with a p-value of 0.0001; between $S_{\perp}$ ≤6 h and $S_{\parallel}$ >6 h, with a p-value of 0.0001; between $S_{\perp}$>6 h and $S_{\parallel}$ ≤6 h, with a p-value of 0.0001; between $S_{\perp}$>6 h and $S_{\parallel}$ >6 h, with a p-value of 0.001.*

This represents a very important result which demonstrates experimentally the anisotropic behaviour of the brain matter in terms of permeability.
The results here presented clearly show that both the infusion rate across the WM tissue and, consequently, its hydraulic permeability are strongly influenced by the tissue intrinsic anisotropy. Previously it has been reported that in WM, the interstitial flow is more rapid in perivascular space and along the axons [Abbott, 2004][Geer and Grossman, 1997]. The results of these experiments suggest a similar mechanism also for a convection driven fluid. In case of $S_{\parallel}$, when the axons are aligned to the injection direction the hydraulic permeability is higher, while in case of $S_{\perp}$, the axons are perpendicular to the fluid, the hydraulic permeability is lower.

4.3 Effect of post-mortem time on the hydraulic permeability

The effect of post-mortem time on the mechanical behaviour of brain tissue has been reported in literature [Garo et al., 2007][Nicolle et al., 2005]. However, not much attention has been paid to the effect of post-mortem time specifically on the hydraulic permeability of brain tissue. One investigation aspect of this thesis is if the hydraulic permeability of the WM changes with post-mortem time. If in the previous section (Sec. 4.2) the analysis was conducted referring to the literature and paying attention to the effect of pressure on the permeability, here the personal considerations of the authors will be argued. So, a different division of the samples will be done and the four groups will be $S_{\parallel} \leq$9 h, $S_{\parallel}$ >9 h, $S_{\perp} \leq$ 9 h, $S_{\perp}$>9 h.

In fact, from the Fig. 4.13, which shows the permeability of $S_{\parallel}$ and $S_{\perp}$ samples measured at different post-mortem times with minimum 3 h and a maximum of 24 h, it emerges that the permeability of both $S_{\parallel}$ and $S_{\perp}$ does not change within the 9 h post-mortem, though there are reasonable fluctuations because of the nature of the biological samples. The weighted mean hydraulic permeability within 9 h post-mortem (calculated with the Eq. 4.1 considering the standard deviation of each group, which, in this case, is identified by the time post-mortem, 3, 4, 5, 6, 7, 8, 9 hour post-mortem) is 3.24×10^{-16} m^2 for $S_{\parallel}$ while that is 0.915×10^{-16} m^2 for $S_{\perp}$.

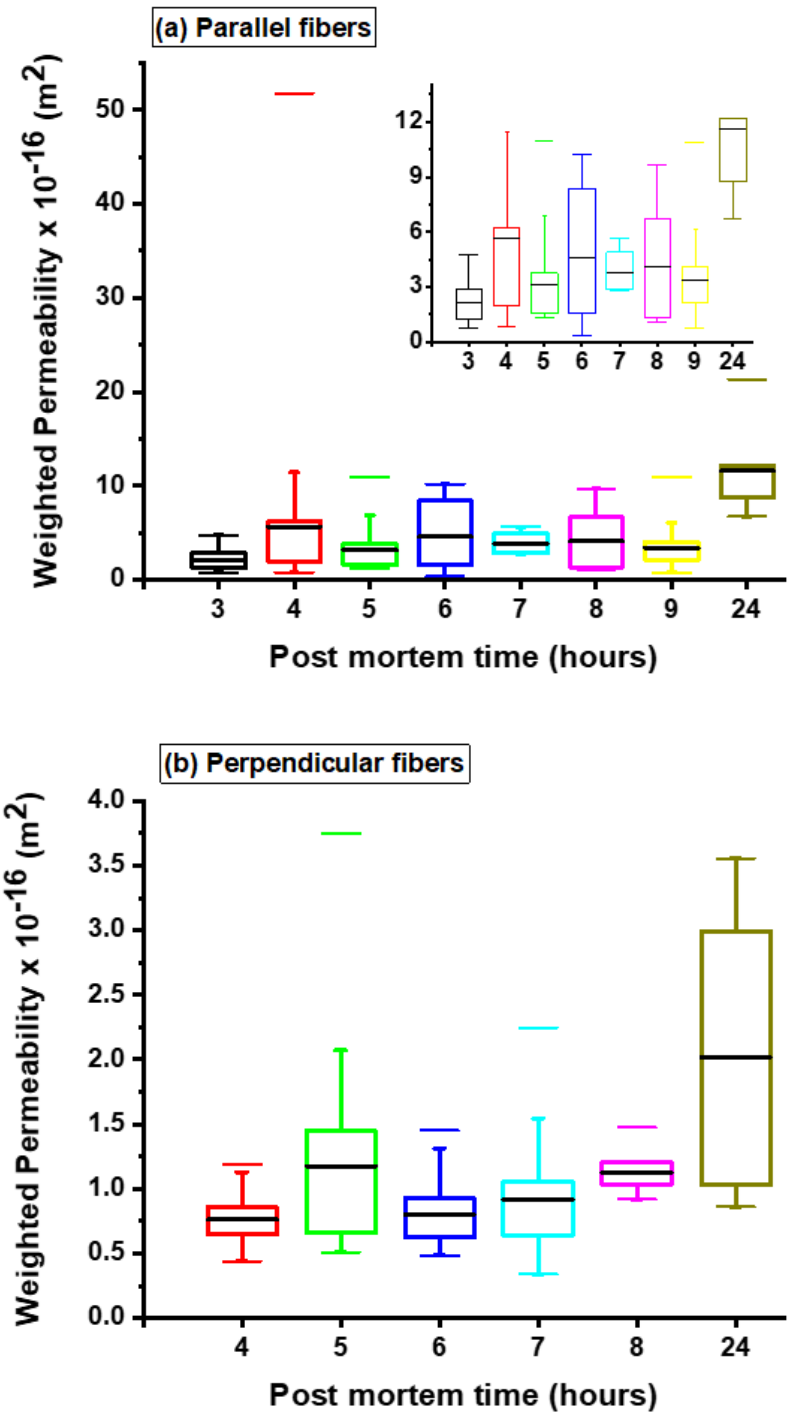

Figure 4.13: *Dependence of hydraulic permeability on the post-mortem time of (a) $S_{\parallel}$ and (b) $S_{\perp}$. The inset shows the corresponding zoomed data. In both cases the permeability does not change within 9 h post-mortem, though there are reasonable fluctuations because of the nature of the biological samples. The measurements at 24 h post-mortem, instead, show a significant difference with respect to the values at/before 9 h post-mortem.*

However, the measurements at 24 h post-mortem time show a significant difference in the permeability of both $S_{\parallel}$ and $S_{\perp}$ samples in comparison to the values at/before 9 h post-mortem time.

The mean permeability of $S_{\parallel}$ at 24 h post-mortem time is about 11.6×10^{-16} m^2 and that of $S_{\perp}$ is about 2.02×10^{-16} m^2. Please note that it was not always possible to run the experiment on $S_{\parallel}$ at higher applied pressure when the post-mortem time was 24 h.

In such scenario, the flow rate at high pressures continues to rise rather reaching a steady state condition, indicative of the potential deterioration of the tissue. Both, $S_{\parallel}$ and $S_{\perp}$ hydraulic permeabilities at different post-mortem times are lognormally distributed as shown in Fig. 4.14 and Fig. 4.15. These measurements clearly demonstrate that with post-mortem time, the WM localised permeability does not change, however, depending on the directionality of axon, its threshold of high pressure to sustain drops. This can be related to the deterioration of the tissue and hence a reason for the changes in mechanical behaviour like stiffness reported in literature.

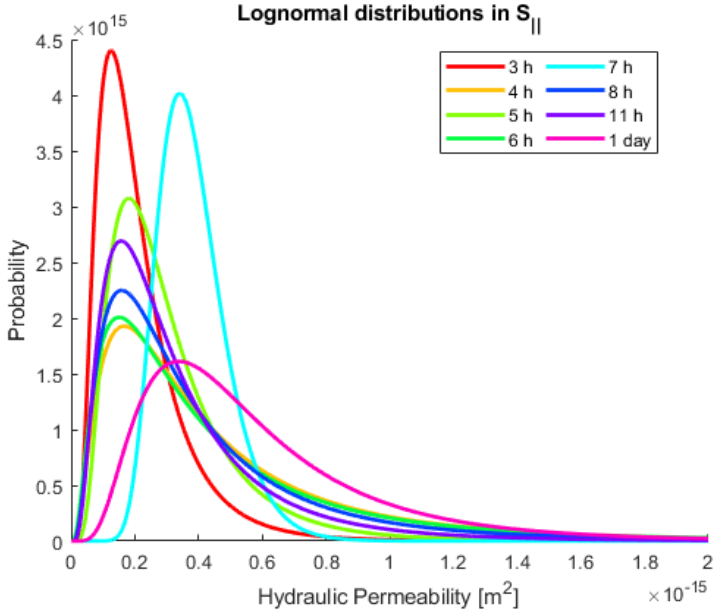

Figure 4.14: *Lognormal distribution of permeability related to post-mortem time in* $S_{\parallel}$.

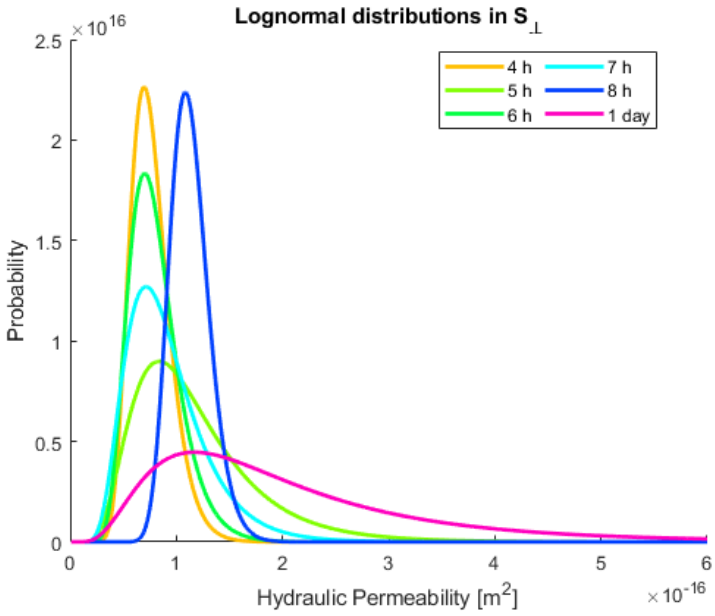

Figure 4.15: *Lognormal distribution of permeability related to post-mortem time in* $S_{\perp}$.

4.4 Comparison with the state of the art

In this study, the hydraulic permeability values of the ovine brain WM are the first experimental determined values, with a direct approach and focusing on the highly anisotropic nature of the WM. In fact, [Franceschini et al., 2006] and [Tavner et al., 2016], in which the permeability of brain tissue was experimentally studied, never considered the directionality in the tissue. Moreover, their reported value of permeability is not the localised permeability of WM.

However, it is fundamental a critic comparison with the other experimental results in literature. Specifically, the value obtained by [Franceschini et al., 2006], $2.42 \cdot 10^{-17}$ m^2, results lower than the thesis authors' conclusion. First of all, this difference can be justified by the fact that their specimens, harvested in order to present an homogeneous tissue, had relatively large dimensions (30 mm of diameter with respect to 5 mm of the samples used in this study) thus including different types of tissue in the same trial. This choice precluded the investigation of possible anisotropy of fluid diffusion. Moreover, a most important consideration is related to their modality to calculate k, resulted from indirect measurements. This limitation is also present in [Tavner et al., 2016], where, even if with a different approach, it has been confirmed the result of [Franceschini et al., 2006]. In [Tavner et al., 2016], an additional issue is the composition

of the specimens, because no distinction between WM and GM has been done.

Nonethless, the results obtained in this thesis represent a real innovation and a significant contribution for the future works.

4.5 Results of the simulations

Since the interest of this study is to infer the main flow direction of the fluid inside the specimen, Fig. 4.16 and Fig. 4.17 show the streamlines in samples with fibres parallel and perpendicular to the needle, respectively. In both cases, even if with different pathways, the fluid starts from the inlet and goes to the lower and to the upper surface of the sample, occupying the whole thickness. Specifically, as the authors expected, in the case of perpendicular fibres, all the injected fluid tends to develop along the Y-axis (direction more permeable) and then exit from the two outlets.

Differently, in the case of the sample with parallel fibres, the fluid immediately goes to both outlets. In both cases, the mass balance between inlet and the two outlets was controlled and results more or less balanced. Specifically, for $S_{\parallel}$ the mass balance is characterised by 2.36 x 10^{-10} kg/s at the inlet, as imposed in the boundary condition, and 6.30 x 10^{-11} kg/s and -2.98 x 10^{-10} kg/s at the outlet_down and at the outlet_up, respectively. In fact the Fig. 4.16 shows the velocity streamlines directed from the inlet to both outlets, with a greater concentration to the outlet_up. Instead, for $S_{\perp}$, the distribution is more balanced, with a mass balance defined by 1.48 x 10^{-10} kg/s at the inlet, -4.67 x 10^{-11} kg/s at the outlet_down, and -1.01 x 10^{-10} kg/s at the outlet_up. Concluding, these results suggest the authors to use the total thickness of the sample in Darcy's law equation, in fact the whole volume of the specimens is involved during these infusions. This consideration is very important, because it demonstrates that the conditions of these experiments are comparable to the theoretical and general situation of application of Darcy's law.

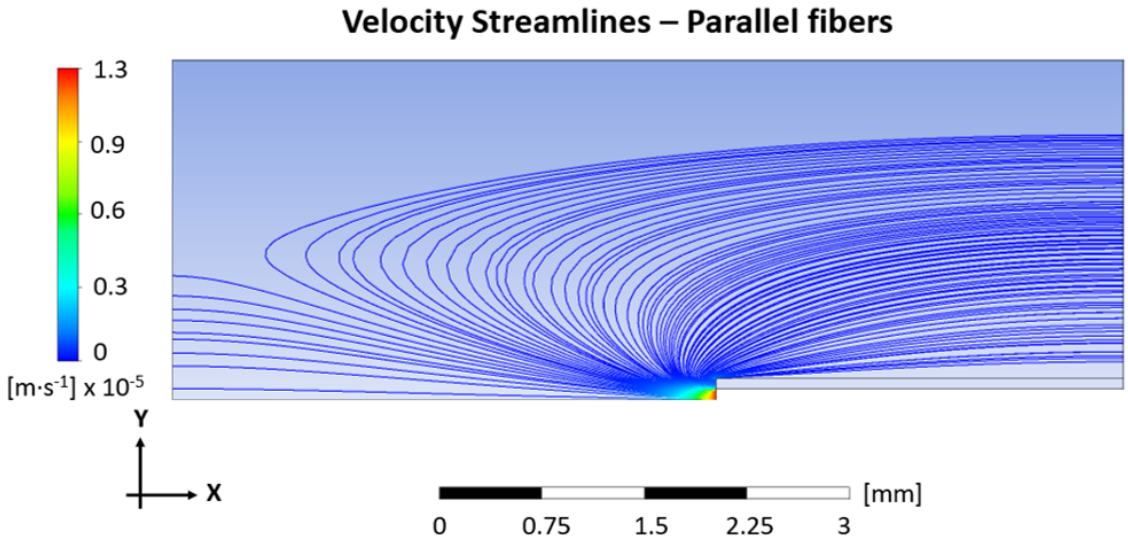

Figure 4.16: *Velocity streamlines in a sample with parallel fibres to X-direction. The particles of fluid injected from the inlet go to both directions (outlet_up and outlet_down), justifying the choice of the authors for the total thickness of the sample in the equation to calculate the hydraulic permeability.*

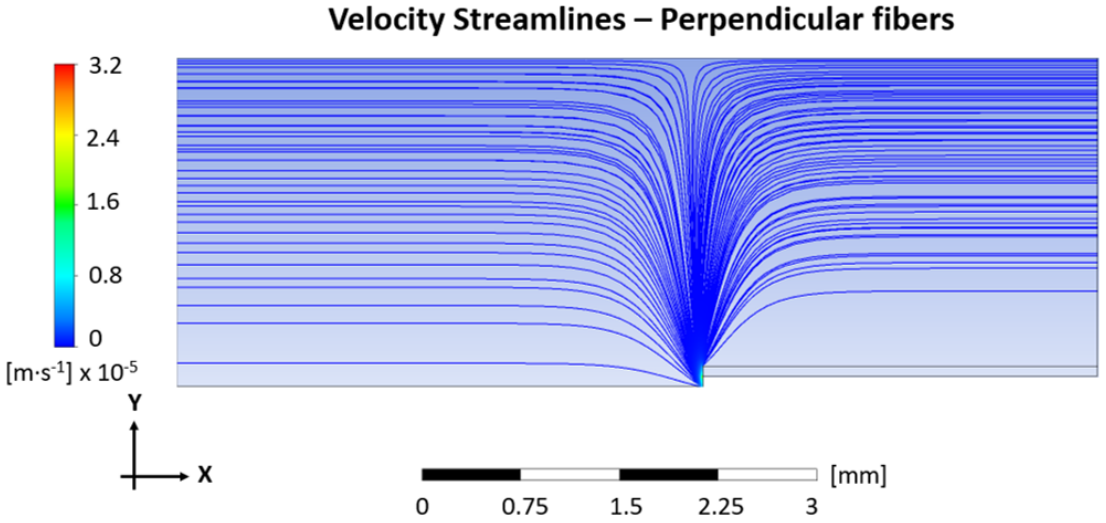

Figure 4.17: *Velocity streamlines in a sample with parallel fibres to Y-direction. The particles of fluid injected from the inlet go to both directions (outlet_up and outlet_down), justifying the choice of the authors for the total thickness of the sample in the equation to calculate the hydraulic permeability.*

Chapter 5

CONCLUSIONS AND FUTURE WORK

In this work the localised hydraulic permeability of cerebral WM was studied for the very first time taking into account its dependence on the anisotropy in the WM. The results, here presented, demonstrate that the hydraulic permeability is significantly higher when the axons in WM are parallel to the flow direction in comparison to that when they are perpendicular to the flow direction. The tissue with axons parallel to flow is more vulnerable to sustain high pressures in contrast to the perpendicular axons which firmly sustain high pressures. Furthermore, the post-mortem time up to 9 h does not change the hydraulic permeability however 24 h post-mortem time makes the tissue more permeable.

These experimental results not only provide a valuable addition to address the issues in technologies like CED but also provide a solid information which can be used to develop a detailed mechanical model for brain tissue.

However in this scenario some limitations must be declared. First of all, we accept that as the perfusions were conducted on post-mortem brain tissue, the current experiments do not fully capture the mechanisms that may influence hydraulic permeability in vivo. This includes the potential effect of innervation, vascular regulation or other local or systemic factors that may influence this parameter. As discussed below, in vivo measurements have their own limitations regarding other aspects that may complicate

measurements of permeability in living animals, but some of these in vivo limitations may be overcome using the *iPerfusion* system.

Moreover during these tests only a few samples have been tested 24 h post-mortem, principally due to the deterioration of the tissue, not allowing a perfect temporal analysis. Besides, only the CR was studied but future works will include a bigger database, with also more samples harvested from different regions of the WM brain tissue. Also the GM will be tested, even if for this one it is not expected a permeability direction dependent. Other aspects about the experimental protocol can be improved, such as not only increasing pressure steps but an analysis of the response of the tissue to a variable applied pressure (increasing steps alternated with decreasing ones, or a decreasing pressure steps).

Appendix A

ANATOMY OF THE BRAIN

Structurally and functionally, the brain can be divided into five parts: cerebrum, cerebellum, midbrain, pons, and medulla oblongata.

In ascending order from the spinal cord, there is the medulla oblongata, which is a sort of passage for ascending and descending nerve fibres. Then, the pons (or bridge), inferiorly connected to the spinal cord through the medulla, links the two cerebellar hemispheres. Within the midbrain, above the pons, there is a narrow cavity, the cerebral aqueduct and many nuclei and bundles of ascending and descending nerve fibres. The medulla, the pons, and the midbrain are known as brainstem. The cerebellum, placed posteriorly to the pons and the medulla oblongata, is traversed by numerous curved sulci, which vary in depth at different parts. The outer cortex is made up of GM while the inner surface consists of WM. Moreover, it is a processing center that is involved in coordination of balance, body position, and the precision and timing of movements.

Finally, the cerebrum, the largest part of the brain, consists of many convoluted ridges (gyri), narrow grooves (sulci), and deep fissures. It is composed of two cerebral hemispheres, (left and right), which are divided by a sagittal fissure, but in the depth, they are connected by a thickly net of nervous fibres, the corpus callosum [Snell, 2010]. In the transverse plane, the corpus callosum extends in radiation of fibres intersecting with bundles of corona radiata fibres [Yakar et al., 2018].

All these nerve fibres constitute the WM of the cerebral hemispheres. They are divided

into three groups according to their connections, commissural fibres, association fibres, and projection fibres [Snell, 2010]:

- **Commissure fibres** connect two corresponding parts of the hemispheres, and they are composed of the anterior, the posterior and the habenular commissure, the fornix and the corpus callosum. The anterior, the posterior and the habenular commissures are small bundles of nerve fibers that cross the midline in the lamina terminalis, the midline immediately above the opening of the cerebral aqueduct and midline in the superior part of the root of the pineal stalk, respectively. The fornix is composed of myelinated nerve fibers and constitutes the efferent system of the hippocampus.
  Finally, the corpus callosum, is the largest commissure of the brain and it is the real connection of the two cerebral hemispheres;

- **Association fibres** connect far and close parts of the same hemisphere, in fact they are divided into short and long groups. The short association fibers run transversely to the long axis of the sulci. The long ones follow different passages because they connect, with three fasciculus, the first motor speech area and the gyri on the inferior surface of the frontal lobe with the cortex of the pole of the temporal lobe, the frontal and parietal lobes with parahippocampal and adjacent temporal cortical regions, and the anterior part of the frontal lobe to the occipital and temporal lobes;

- **Projection fibres** connect cortex to the brainstem and the thalamus in afferent and efferent ways. These radiating projection fibres are called corona radiata.

In the cerebral matter, a multitude of cells coexists; they can be classified into neurons and non-neurons (namely glia-cells) [von Bartheld et al., 2016]. Neurons present a body and neurites (called dendrites, if they are responsible for the transfer of information toward the cell body, or if they consist in one single tubule, it is named axon, embedded of myelin sheat to conduct impulses away from the cell) [Snell, 2010]. Glia-cells, instead, are smaller than neurons and they don't have the myelinated portion [Richardson et al., 2006].

The exchange of nutrients between these cells and the blood is guaranteed by extracellular space [Snell, 2010]. In particular, endothelial cells of the BBB allow the transport of ions and solutes [Guerra et al., 2017]. The permeability of the BBB is related to the size and the lipid solubility of the molecules; in the specific, plasma proteins and other large molecules do not pass, instead of gases and water pass through the barrier [Snell, 2010].

Appendix B

HYDROGEL PERMEABILITY

Mechanically accurate synthetic tissues (also known as phantom) are popular materials for biological and biomedical applications. Since they exhibit properties similar to natural tissues, reproducing their deformation pattern and mechanical response, their applicability extends into several scientific fields, such as surgical training, prosthesis design, testing haptic devices and performing sensor calibrations, and impact tests and trauma analysis [Forte et al., 2016]. However, cadaveric training is still considered the gold standard in order to achieve technical proficiency [Holland et al., 2011] but the animal models are perfect replacements [Leong et al., 2008], unfortunately with not a few drawbacks: anatomic structures different from human specimens, ethical restrictions and the necessity of specific equipment.

In this contest, a synthetic material, simple to prepare, inexpensive and able to mimic the three mechanical properties (stiffness, toughness and needle-tissue frictional interaction) of the brain [Forte et al., 2016][Tan et al., 2018] was used to test also its hydraulic permeability and to compare the values with the results obtained on the ovine tissue.

The material in question is the composite hydrogel (CH) developed by Forte et al. to match the complex viscoelastic behaviour of the brain [Forte et al., 2016] and then improved by Tan et al. to include also the cutting and the friction between brain and needle [Tan et al., 2018]. The experiments with *iPerfusion* confirmed that the last version of the CH shows also a permeability comparable to the real biologic tissue.

Moreover, a few additional tests were performed on the CH, on which the concentrations of the components were slightly changed in order to try to justify eventual relationships between the studied parameter and the quantities of PVA and PHY. The original CH was prepared using 2.5wt% poly(vinyl) alcohol (PVA) (molecular weight 146,000–186,000 Da) and 1.1wt% phytagel (PHY) accurately dissolved separately in deionised water for 1 h al 90 °C. The separate solutions were combined in a 1:1 weight ratio and stirred at 70°C for an additional 30 min. The mixed solution, poured into a petri dish and cooled down at room temperature, was frozen and stored at -25°C for 15 h, allowing the physical cross-linking by hydrogen bonds. Before samples preparation and testing, the petri dish was thawed to room temperature in a controlled environment (about 19°C). The second solution was similarly prepared, with the only difference in the composition: 5wt% PVA and 0.6wt% PHY.
Following the same protocol proposed in this thesis to test the ovine tissue, explained in Sec. 3.2, cylindrical samples of about 5 mm of diameter and about 7 mm height were cut from petri dish bulk material using the same plastic tube (pipette) as the brain samples. The hydrogel samples were kept hydrated before and during testing, completely immersed into deionised water, the same used for the injection.

For the purpose of measuring the hydraulic permeability using the apparatus test described in Sec. 3.3, the needle (BD Microlance Stainless Steel Needles; 30G x ½”; $0,3$ x 13 mm) was inserted for about 4 mm of the thickness of the samples. The tests were performed with the same experimental protocol applied to the brain and widely discussed in Sec. 3.4. Briefly, an 8 pressure-steps protocol, from 7 to 25 $mmHg$, was imposed, the internal flow rate was measured, and the hydraulic permeability was calculated exploring Darcy’s law (Eq. 2.1). This analogy with the experiments conducted on the ovine tissue allowed the authors to make a sort of comparison between the two materials.

Although the results are promising, the CH is not able to mimic the interior disposition of the fibres, vaguely replicated from a randomly cross-linking. For this reason, no considerations can be done about the anisotropy of the brain tissue, not present in the CH. The obtained values demonstrate that the CH is most similar to the samples with parallel fibres with respect to the direction of the needle than the samples with

perpendicular ones. Specifically, the average values for CH_1 (2.5wt% and 1.1wt%) and CH_2 (5wt% and 0.6wt%) are $2.49 \cdot 10^{-16}$ m^2 and $3.55 \cdot 10^{-16}$ m^2, respectively. These measurements, so similar to the real biologic tissue, open important opportunities for the realisation of surgical planning and training devices and tools for in-vitro tissue testing.

ABBREVIATIONS

- ACSF: Artificial cerebrospinal fluid
- BBB: Blood-brain barrier
- CED: Convection-enhanced delivery
- CH: Composite hydrogel
- CNS: Central nervous system
- CR: Corona radiata
- CSF: Cerebrospinal fluid
- DMEM: Dulbecco's modified eagle medium
- DTI: Diffusion tensor imaging
- DW-MRI: Diffusion-weighted magnetic resonance image
- ECM: Extra cellular matrix
- EDEN2020: Enhanced Delivery Ecosystem for Neurosurgery in 2020
- FEM: Finite element method
- GAG: Glycosaminoglycans

- GB: Glioblastoma
- GBM: Glioblastoma multiforme
- GBM-PNC: Glioblastoma with primitive neuronal components
- GM: Grey matter
- LVDT: Linear variable displacement transducer
- MCL: Medial collateral ligament
- MRI: Magnetic resonance imaging
- PBS: phosphate-buffered saline
- PGMA: Propylene glycol methyl acetate
- PHY: Phytagel
- PVA: Poly(vynyl) alcohol
- ROI: Region of interest
- RT: Radiation therapy
- TMZ: Temozolomide
- WHO: World Health Organization
- WM: White matter

Bibliography

[Abbott, 2004] Abbott, N. (2004). Evidence for bulk flow of brain interstitial fluid: significance for physiology and pathology. *Neurochemistry International*, 45(4):545–552.

[Aihara et al., 2003] Aihara, M., Lindsey, J. D., and Weinreb, R. N. (2003). Aqueous Humor Dynamics in Mice. *Investigative Opthalmology & Visual Science*, 44(12):5168.

[Alam et al., 2010] Alam, M. I., Beg, S., Samad, A., Baboota, S., Kohli, K., Ali, J., Ahuja, A., and Akbar, M. (2010). Strategy for effective brain drug delivery. *European Journal of Pharmaceutical Sciences*, 40(5):385–403.

[Alexander et al., 2019] Alexander, D. C., Dyrby, T. B., Nilsson, M., and Zhang, H. (2019). Imaging brain microstructure with diffusion MRI: practicality and applications. *NMR in Biomedicine*, 32(4):e3841.

[Andriakopoulou et al., 2018] Andriakopoulou, C., Zadpoor, A., Grant, M., and Riches, P. (2018). Development and mechanical characterisation of self-compressed collagen gels. *Materials Science and Engineering: C*, 84(October 2017):243–247.

[ANSYS, 2017] ANSYS (2017). ANSYS Fluent theory guide.

[Anton et al., 2012] Anton, K., Baehring, J. M., and Mayer, T. (2012). Glioblastoma Multiforme. *Hematology/Oncology Clinics of North America*, 26(4):825–853.

[Arifin et al., 2009] Arifin, D. Y., Lee, K. Y. T., Wang, C.-H., and Smith, K. A. (2009). Role of Convective Flow in Carmustine Delivery to a Brain Tumor. *Pharmaceutical Research*, 26(10):2289–2302.

[Barany, 1964] Barany, E. H. (1964). Simultaneous Measurement of Changing Intraocular Pressure and Outflow Facility in the Vervet Monkey By Constant Pressure Infusion. *Investigative ophthalmology*, 3:135–13543.

[Barry and Aldis, 1990] Barry, S. and Aldis, G. (1990). Comparison of models for flow induced deformation of soft biological tissue. *Journal of Biomechanics*, 23(7):647–654.

[Basser, 1992] Basser, P. J. (1992). Interstitial pressure, volume, and flow during infusion into brain tissue. *Microvascular Research*, 44(2):143–165.

[Bobo et al., 1994] Bobo, R. H., Laske, D. W., Akbasak, A., Morrison, P. F., Dedrick, R. L., and Oldfield, E. H. (1994). Convection-enhanced delivery of macromolecules in the brain. *Proceedings of the National Academy of Sciences*, 91(6):2076–2080.

[Brem et al., 1995] Brem, H., Piantadosi, S., Burger, P., Walker, M., Selker, R., Vick, N., Black, K., Sisti, M., Brem, S., Mohr, G., Muller, P., Morawetz, R., and Schold, S. (1995). Placebo-controlled trial of safety and efficacy of intraoperative controlled delivery by biodegradable polymers of chemotherapy for recurrent gliomas. *The Lancet*, 345(8956):1008–1012.

[Budday et al., 2015] Budday, S., Nay, R., de Rooij, R., Steinmann, P., Wyrobek, T., Ovaert, T. C., and Kuhl, E. (2015). Mechanical properties of gray and white matter brain tissue by indentation. *Journal of the Mechanical Behavior of Biomedical Materials*, 46:318–330.

[Burmister, 1955] Burmister, D. M. (1955). Principles of Permeability Testing of Soils. In *Symposium on Permeability of Soils*, pages 3–3–24. ASTM International, 100 Barr Harbor Drive, PO Box C700, West Conshohocken, PA 19428-2959.

[Chatelin et al., 2010] Chatelin, S., Constantinesco, A., and Willinger, R. (2010). Fifty years of brain tissue mechanical testing: From in vitro to in vivo investigations. *Biorheology*, 47(5-6):255–276.

[Chen et al., 1999] Chen, M. Y., Lonser, R. R., Morrison, P. F., Governale, L. S., and Oldfield, E. H. (1999). Variables affecting convection-enhanced delivery to the striatum: a systematic examination of rate of infusion, cannula size, infusate concentration, and tissue—cannula sealing time. *Journal of Neurosurgery*, 90(2):315–320.

[Cheng and Bilston, 2007] Cheng, S. and Bilston, L. E. (2007). Unconfined compression of white matter. *Journal of Biomechanics*, 40(1):117–124.

[Chor and Li, 2007] Chor, M. V. and Li, W. (2007). A permeability measurement system for tissue engineering scaffolds. *Measurement Science and Technology*, 18(1):208–216.

[Darvish and Crandall, 2001] Darvish, K. and Crandall, J. (2001). Nonlinear viscoelastic effects in oscillatory shear deformation of brain tissue. *Medical Engineering & Physics*, 23(9):633–645.

[Datta, 2006] Datta, A. K. (2006). Hydraulic permeability of food tissues. *International Journal of Food Properties*, 9(4):767–780.

[Engelhard, 2000] Engelhard, H. H. (2000). The role of interstitial BCNU chemotherapy in the treatment of malignant glioma. *Surgical Neurology*, 53(5):458–464.

[Fireman, 1944] Fireman, M. (1944). Permeability measurements on disturbed soil samples. *Soil Science*, 58(5):337–354.

[Fischbarg et al., 1980] Fischbarg, J., Hofer, G. L., and Koatz, R. A. (1980). Priming of the fluid pump by osmotic gradients across rabbit corneal endothelium. *Biochimica et Biophysica Acta (BBA) - Biomembranes*, 603(1):198–206.

[Forte et al., 2016] Forte, A. E., Galvan, S., Manieri, F., Rodriguez y Baena, F., and Dini, D. (2016). A composite hydrogel for brain tissue phantoms. *Materials & Design*, 112:227–238.

[Franceschini et al., 2006] Franceschini, G., Bigoni, D., Regitnig, P., and Holzapfel, G. A. (2006). Brain tissue deforms similarly to filled elastomers and follows consolidation theory. *Journal of the Mechanics and Physics of Solids*, 54(12):2592–2620.

[Garo et al., 2007] Garo, A., Hrapko, M., Van Dommelen, J. A. W., and Peters, G. W. M. (2007). Towards a reliable characterisation of the mechanical behaviour of brain tissue: The effects of post-mortem time and sample preparation. *Biorheology*, 44(1):51–58.

[Geer and Grossman, 1997] Geer, C. P. and Grossman, S. A. (1997). Interstitial fluid flow along white matter tracts : A potentially important mechanism for the dissemination of primary brain tumors. pages 193–201.

[Griffin et al., 2016] Griffin, M., Premakumar, Y., Seifalian, A., Butler, P. E., and Szarko, M. (2016). Biomechanical Characterization of Human Soft Tissues Using Indentation and Tensile Testing. *Journal of Visualized Experiments*, 2016(118):1–8.

[Groothuis, 2000] Groothuis, D. R. (2000). The blood-brain and blood-tumor barriers: A review of strategies for increasing drug delivery. *Neuro-Oncology*, 2(1):45–59.

[Gu et al., 1999] Gu, W. Y., Mao, X. G., Foster, R. J., Weidenbaum, M., Mow, V. C., and Rawlins, B. A. (1999). The Anisotropic Hydraulic Permeability of Human Lumbar Anulus Fibrosus. *Spine*, 24(23):2449.

[Gu and Yao, 2003] Gu, W. Y. and Yao, H. (2003). Effects of hydration and fixed charge density on fluid transport in charged hydrated soft tissues. *Annals of Biomedical Engineering*, 31(10):1162–1170.

[Guerra et al., 2017] Guerra, M., Blázquez, J. L., and Rodríguez, E. M. (2017). Blood–brain barrier and foetal-onset hydrocephalus, with a view on potential novel treatments beyond managing CSF flow. *Fluids and Barriers of the CNS*, 14(1):19.

[Heneghan and Riches, 2008] Heneghan, P. and Riches, P. E. (2008). Determination of the strain-dependent hydraulic permeability of the compressed bovine nucleus pulposus. *Journal of Biomechanics*, 41(4):903–906.

[Holland et al., 2011] Holland, J. P., Waugh, L., Horgan, A., Paleri, V., and Deehan, D. J. (2011). Cadaveric Hands-on Training for Surgical Specialties: Is This Back to the Future for Surgical Skills Development? *Journal of Surgical Education*, 68(2):110–116.

[Holm et al., 1981] Holm, S., Maroudas, A., Urban, J. P. G., Selstam, G., and Nachemson, A. (1981). Nutrition of the Intervertebral Disc: Solute Transport and Metabolism. *Connective Tissue Research*, 8(2):101–119.

[Holmes, 1985] Holmes, M. H. (1985). A theoretical analysis for determining the nonlinear hydraulic permeability of a soft tissue from a permeation experiment. *Bulletin of Mathematical Biology*, 47(5):669–683.

[Huang et al., 1997] Huang, Y., Rumschitzki, D., Chien, S., and Weinbaum, S. (1997). A fiber matrix model for the filtration through fenestral pores in a compressible arterial intima. *American Journal of Physiology-Heart and Circulatory Physiology*, 272(4):H2023–H2039.

[Innocentini et al., 2010] Innocentini, M. D. M., Faleiros, R. K., Pisani, R., Thijs, I., Luyten, J., and Mullens, S. (2010). Permeability of porous gelcast scaffolds for bone tissue engineering. *Journal of Porous Materials*, 17(5):615–627.

[Isogai et al., 1983] Isogai, Y., Nose, H., Miki, K., and Morimoto, T. (1983). Dynamics of fluid movement between intravascular and interstitial spaces. *Journal of Theoretical Biology*, 100(2):305–317.

[Kaczmarek et al., 1997] Kaczmarek, M., Subramaniam, R. P., and Neff, S. R. (1997). The hydromechanics of hydrocephalus: Steady-state solutions for cylindrical geometry. *Bulletin of Mathematical Biology*, 59(2):295–323.

[Kalyanasundaram et al., 1997] Kalyanasundaram, S., Calhoun, V. D., and Leong, K. W. (1997). A finite element model for predicting the distribution of drugs delivered intracranially to the brain. *American Journal of Physiology-Regulatory, Integrative and Comparative Physiology*, 273(5):R1810–R1821.

[Kapellos and Alexiou, 2013] Kapellos, G. E. and Alexiou, T. S. (2013). Modeling Momentum and Mass Transport in Cellular Biological Media: From the Molecular to the Tissue Scale. In *Transport in Biological Media*, number May 2013, pages 1–40. Elsevier.

[Katz et al., 1982] Katz, D., Tam, P., Berger, S., and Sensabaugh, G. (1982). Flow permeation analysis of bovine cervical mucus. *Biophysical Journal*, 38(2):153–159.

[Kirson et al., 2007] Kirson, E. D., Dbaly, V., Tovarys, F., Vymazal, J., Soustiel, J. F., Itzhaki, A., Mordechovich, D., Steinberg-Shapira, S., Gurvich, Z., Schneiderman, R., Wasserman, Y., Salzberg, M., Ryffel, B., Goldsher, D., Dekel, E., and Palti, Y. (2007). Alternating electric fields arrest cell proliferation in animal tumor models and human brain tumors. *Proceedings of the National Academy of Sciences*, 104(24):10152–10157.

[Kirson et al., 2009] Kirson, E. D., Schneiderman, R. S., Dbalý, V., Tovaryš, F., Vymazal, J., Itzhaki, A., Mordechovich, D., Gurvich, Z., Shmueli, E., Goldsher, D., Wasserman, Y., and Palti, Y. (2009). Chemotherapeutic treatment efficacy and sensitivity are increased by adjuvant alternating electric fields (TTFields). *BMC Medical Physics*, 9(1):1.

[Klanchar and Tarbell, 1987] Klanchar, M. and Tarbell, J. (1987). Modeling water flow through arterial tissue. *Bulletin of Mathematical Biology*, 49(6):651–669.

[Kumar et al., 2013] Kumar, S., Shah, S., Tang, H. M., Smith, M., Borrás, T., and Danias, J. (2013). Tissue Plasminogen Activator in Trabecular Meshwork Attenuates Steroid Induced Outflow Resistance in Mice. *PLoS ONE*, 8(8):e72447.

[Lai and Mow, 1980] Lai, W. M. and Mow, V. C. (1980). Drag-induced compression of articular cartilage during a permeation experiment1. *Biorheology*, 17(1-2):111–123.

[Leong et al., 2008] Leong, J. J. H., Leff, D. R., Das, A., Aggarwal, R., Reilly, P., Atkinson, H. D. E., Emery, R. J., and Darzi, A. W. (2008). Validation of orthopaedic bench models for trauma surgery. *The Journal of Bone and Joint Surgery. British volume*, 90-B(7):958–965.

[Lidar et al., 2004] Lidar, Z., Mardor, Y., Jonas, T., Pfeffer, R., Faibel, M., Nass, D., Hadani, M., and Ram, Z. (2004). Convection-enhanced delivery of paclitaxel for the treatment of recurrent malignant glioma: a Phase I/II clinical study. *Journal of Neurosurgery*, 100(3):472–479.

[Louis et al., 2016] Louis, D. N., Perry, A., Reifenberger, G., von Deimling, A., Figarella-Branger, D., Cavenee, W. K., Ohgaki, H., Wiestler, O. D., Kleihues, P., and Ellison, D. W. (2016). The 2016 World Health Organization Classification of Tumors of the Central Nervous System: a summary. *Acta Neuropathologica*, 131(6):803–820.

[Lu and Mow, 2008] Lu, X. L. and Mow, V. C. (2008). Biomechanics of Articular Cartilage and Determination of Material Properties. *Medicine & Science in Sports & Exercise*, 40(2):193–199.

[Mansour and Mow, 1976] Mansour, J. M. and Mow, V. C. (1976). The permeability of articular cartilage under compressive strain and at high pressures. *The Journal of bone and joint surgery. American volume*, 58(4):509–16.

[McElhaney et al., 1973] McElhaney, J. H., Melvin, J. W., Roberts, V. L., and Portnoy, H. D. (1973). Dynamic Characteristics of the Tissues of the Head. In *Perspectives in Biomedical Engineering*, pages 215–222. Palgrave Macmillan UK, London.

[Mehta et al., 2015] Mehta, A. I., Linninger, A., Lesniak, M. S., and Engelhard, H. H. (2015). Current status of intratumoral therapy for glioblastoma. *Journal of Neuro-Oncology*, 125(1):1–7.

[Metz et al., 1970] Metz, H., McElhaney, J., and Ommaya, A. K. (1970). A comparison of the elasticity of live, dead, and fixed brain tissue. *Journal of Biomechanics*, 3(4):453–458.

[Miga et al., 2000] Miga, M. I., Paulsen, K. D., Hoopes, P. J., Kennedy, F. E., Hartov, A., and Roberts, D. W. (2000). In Vivo Modeling of Interstitial Pressure in the Brain Under

Surgical Load Using Finite Elements. *Journal of Biomechanical Engineering*, 122(4):354–363.

[Milhorat, 1972] Milhorat, T. (1972). *Hydrocephalus and the Cerebrospinal Fluid.* The Williams and Wilkins Company, Baltimore.

[Mlekoday, 1983] Mlekoday, H. J. (1983). Osmotic water permeability of the human red cell. Dependence on direction of water flow and cell volume. *The Journal of General Physiology*, 81(2):213–220.

[Mohsen et al., 2013] Mohsen, L. A., Shi, V., Jena, R., Gillard, J. H., and Price, S. J. (2013). Diffusion tensor invasive phenotypes can predict progression-free survival in glioblastomas. *British Journal of Neurosurgery*, 27(4):436–441.

[Morrison et al., 1994] Morrison, P. F., Laske, D. W., Bobo, H., Oldfield, E. H., and Dedrick, R. L. (1994). High-flow microinfusion: Tissue penetration and pharmacodynamics. *American Journal of Physiology - Regulatory Integrative and Comparative Physiology*, 266(1 35-1).

[Mow et al., 1998] Mow, V. C., Ateshian, G. A., Lai, W. M., and Gu, W. Y. (1998). Effects of Fixed Charges on the Stress- Relaxation Behavior of Hydrated. 35(98):4945–4962.

[Mow et al., 1984] Mow, V. C., Holmes, M. H., and Michael Lai, W. (1984). Fluid transport and mechanical properties of articular cartilage: A review. *Journal of Biomechanics*, 17(5):377–394.

[Mow et al., 1980] Mow, V. C., Kuei, S. C., Lai, W. M., and Armstrong, C. G. (1980). Biphasic Creep and Stress Relaxation of Articular Cartilage in Compression: Theory and Experiments. *Journal of Biomechanical Engineering*, 102(1):73–84.

[Muldoon et al., 1995] Muldoon, L. L., Nilaver, G., Kroll, R. A., Pagel, M. A., Breakefield, X. O., Chiocca, E. A., Davidson, B. L., Weissleder, R., and Neuwelt, E. A. (1995). Comparison of intracerebral inoculation and osmotic blood-brain barrier disruption for delivery of adenovirus, herpesvirus, and iron oxide particles to normal rat brain. *American Journal of Pathology*, 147(6):1840–1851.

[Nagle and Scott, 1978] Nagle, J. and Scott, H. (1978). Lateral compressibility of lipid mono- and bilayers. Theory of membrane permeability. *Biochimica et Biophysica Acta (BBA) - Biomembranes*, 513(2):236–243.

[Naidich et al., 2016] Naidich, T. P., Krayenbühl, N., Kollias, S., Bou-Haidar, Pascal Bluestone, A. Y., and Carpenter, D. M. (2016). White matter.

[Netti et al., 2000] Netti, P. A., Berk, D. A., Swartz, M. A., Grodzinsky, A. J., and Jain, R. K. (2000). Role of extracellular matrix assembly in interstitial transport in solid tumors. *Cancer Research*, 60(9):2497–2503.

[Nicolle et al., 2004] Nicolle, S., Lounis, M., and Willinger, R. (2004). Shear Properties of Brain Tissue over a Frequency Range Relevant for Automotive Impact Situations: New Experimental Results. In *SAE Technical Papers*, volume 2004-Novem, pages 239–258.

[Nicolle et al., 2005] Nicolle, S., Lounis, M., Willinger, R., and Palierne, J. F. (2005). Shear linear behavior of brain tissue over a large frequency range. *Biorheology*, 42(3):209–223.

[O'Brien et al., 2006] O'Brien, F. J., Harley, B. A., Waller, M. A., Yannas, I. V., Gibson, L. J., and Prendergast, P. J. (2006). The effect of pore size on permeability and cell attachment in collagen scaffolds for tissue engineering. *Technology and Health Care*, 15(1):3–17.

[Ochoa et al., 2009] Ochoa, I., Sanz-Herrera, J. A., García-Aznar, J. M., Doblaré, M., Yunos, D. M., and Boccaccini, A. R. (2009). Permeability evaluation of 45S5 Bioglass®-based scaffolds for bone tissue engineering. *Journal of Biomechanics*, 42(3):257–260.

[O'Donnell and Westin, 2011] O'Donnell, L. J. and Westin, C.-F. (2011). An Introduction to Diffusion Tensor Image Analysis. *Neurosurgery Clinics of North America*, 22(2):185–196.

[Ostrom et al., 2013] Ostrom, Q. T., Gittleman, H., Farah, P., Ondracek, A., Chen, Y., Wolinsky, Y., Stroup, N. E., Kruchko, C., and Barnholtz-Sloan, J. S. (2013). CBTRUS Statistical Report: Primary Brain and Central Nervous System Tumors Diagnosed in the United States in 2006-2010. *Neuro-Oncology*, 15(suppl 2):ii1–ii56.

[Ouyang et al., 2013] Ouyang, H., Nauman, E., and Shi, R. (2013). Contribution of cytoskeletal elements to the axonal mechanical properties. *Journal of Biological Engineering*, 7(1):21.

[Parker et al., 1987] Parker, K. H., Mehta, R. V., and Caro, C. G. (1987). Steady flow in porous, elastically deformable materials. *Journal of Applied Mechanics, Transactions ASME*, 54(4):794–800.

[Pearce et al., 2017] Pearce, A., Haas, M., Viney, R., Pearson, S.-A., Haywood, P., Brown, C., and Ward, R. (2017). Incidence and severity of self-reported chemotherapy side effects in routine care: A prospective cohort study. *PLOS ONE*, 12(10):e0184360.

[Pennella et al., 2013] Pennella, F., Cerino, G., Massai, D., Gallo, D., Falvo D'Urso Labate, G., Schiavi, A., Deriu, M. A., Audenino, A., and Morbiducci, U. (2013). A Survey of Methods for the Evaluation of Tissue Engineering Scaffold Permeability. *Annals of Biomedical Engineering*, 41(10):2027–2041.

[Pieri et al., 2019] Pieri, V., Trovatelli, M., Cadioli, M., Zani, D. D., Brizzola, S., Ravasio, G., Acocella, F., Di Giancamillo, M., Malfassi, L., Dolera, M., Riva, M., Bello, L., Falini, A., and Castellano, A. (2019). In vivo Diffusion Tensor Magnetic Resonance Tractography of the Sheep Brain: An Atlas of the Ovine White Matter Fiber Bundles. *Frontiers in Veterinary Science*, 6(October):1–15.

[Quinn et al., 2009] Quinn, J. A., Jiang, S. X., Carter, J., Reardon, D. A., Desjardins, A., Vredenburgh, J. J., Rich, J. N., Gururangan, S., Friedman, A. H., Bigner, D. D., Sampson, J. H., McLendon, R. E., Herndon, J. E., Threatt, S., and Friedman, H. S. (2009). Phase II Trial of Gliadel plus O6-Benzylguanine in Adults with Recurrent Glioblastoma Multiforme. *Clinical Cancer Research*, 15(3):1064–1068.

[Raghavan et al., 2016] Raghavan, R., Brady, M. L., and Sampson, J. H. (2016). Delivering therapy to target: improving the odds for successful drug development. *Therapeutic Delivery*, 7(7):457–481.

[Reulen et al., 1977] Reulen, H. J., Graham, R., Spatz, M., and Klatzo, I. (1977). Role of pressure gradients and bulk flow in dynamics of vasogenic brain edema. *Journal of Neurosurgery*, 46(1):24–35.

[Reynaud and Quinn, 2006] Reynaud, B. and Quinn, T. M. (2006). Anisotropic hydraulic permeability in compressed articular cartilage. *Journal of Biomechanics*, 39(1):131–137.

[Richardson et al., 2006] Richardson, W. D., Kessaris, N., and Pringle, N. (2006). Oligodendrocyte wars. *Nature Reviews Neuroscience*, 7(1):11–18.

[Sampson et al., 2011] Sampson, J. H., Brady, M., Raghavan, R., Mehta, A. I., Friedman, A. H., Reardon, D. A., Petry, N. A., Barboriak, D. P., Wong, T. Z., Zalutsky, M. R., Lally-Goss, D., and Bigner, D. D. (2011). Colocalization of gadolinium-diethylene triamine pen-

taacetic acid with high-molecular-weight molecules after intracerebral convection-enhanced delivery in humans. *Neurosurgery*, 69(3):668–676.

[Santamaría et al., 2012] Santamaría, V. A., Deplaine, H., Mariggió, D., Villanueva-Molines, A., García-Aznar, J., Ribelles, J. G., Doblaré, M., Ferrer, G. G., and Ochoa, I. (2012). Influence of the macro and micro-porous structure on the mechanical behavior of poly(l-lactic acid) scaffolds. *Journal of Non-Crystalline Solids*, 358(23):3141–3149.

[Schiavi et al., 2012] Schiavi, A., Guglielmone, C., Pennella, F., and Morbiducci, U. (2012). Acoustic method for permeability measurement of tissue-engineering scaffold. *Measurement Science and Technology*, 23(10):105702.

[Setton et al., 1993] Setton, L. A., Zhu, W., and Mow, V. C. (1993). The biphasic poroviscoelastic behavior of articular cartilage: Role of the surface zone in governing the compressive behavior. *Journal of Biomechanics*, 26(4-5):581–592.

[Shen et al., 2006] Shen, F., Tay, T. E., Li, J. Z., Nigen, S., Lee, P. V. S., and Chan, H. K. (2006). Modified Bilston Nonlinear Viscoelastic Model for Finite Element Head Injury Studies. *Journal of Biomechanical Engineering*, 128(5):797–801.

[Sherwood et al., 2016] Sherwood, J. M., Reina-Torres, E., Bertrand, J. A., Rowe, B., and Overby, D. R. (2016). Measurement of outflow facility using iPerfusion. *PLoS ONE*, 11(3):1–29.

[Shimko and Nauman, 2007] Shimko, D. A. and Nauman, E. A. (2007). Development and characterization of a porous poly(methyl methacrylate) scaffold with controllable modulus and permeability. *Journal of Biomedical Materials Research Part B: Applied Biomaterials*, 80B(2):360–369.

[Snell, 2010] Snell, R. S. (2010). *Clinical Neuroanatomy*. 7th edition.

[Støverud et al., 2012] Støverud, K. H., Darcis, M., Helmig, R., and Hassanizadeh, S. M. (2012). Modeling Concentration Distribution and Deformation During Convection-Enhanced Drug Delivery into Brain Tissue. *Transport in Porous Media*, 92(1):119–143.

[Stummer et al., 2006] Stummer, W., Pichlmeier, U., Meinel, T., Wiestler, O. D., Zanella, F., and Reulen, H.-J. (2006). Fluorescence-guided surgery with 5-aminolevulinic acid for resection of malignant glioma: a randomised controlled multicentre phase III trial. *The Lancet Oncology*, 7(5):392–401.

[Stupp et al., 2005] Stupp, R., Mason, W. P., and van den Bent, M. J. (2005). "Radiotherapy plus Concomitant and Adjuvant Temozolomide for Glioblastoma". *Oncology Times*, 27(9):15–16.

[Swabb et al., 1974] Swabb, E., J., W., and Gullino, P. (1974). Diffusion and Convection in Normal and Neoplastic Tissues. *Cancer Research*, 34(10):2814–2822.

[Swider et al., 2007] Swider, P., Conroy, M., Pédrono, A., Ambard, D., Mantell, S., Søballe, K., and Bechtold, J. E. (2007). Use of high-resolution MRI for investigation of fluid flow and global permeability in a material with interconnected porosity. *Journal of Biomechanics*, 40(9):2112–2118.

[Tan et al., 2018] Tan, Z., Dini, D., Rodriguez y Baena, F., and Forte, A. E. (2018). Composite hydrogel: A high fidelity soft tissue mimic for surgery. *Materials & Design*, 160:886–894.

[Tavner et al., 2016] Tavner, A. C., Roy, T. D., Hor, K. W., Majimbi, M., Joldes, G. R., Wittek, A., Bunt, S., and Miller, K. (2016). On the appropriateness of modelling brain parenchyma as a biphasic continuum. *Journal of the Mechanical Behavior of Biomedical Materials*, 61:511–518.

[Truscello et al., 2012] Truscello, S., Kerckhofs, G., Van Bael, S., Pyka, G., Schrooten, J., and Van Oosterwyck, H. (2012). Prediction of permeability of regular scaffolds for skeletal tissue engineering: A combined computational and experimental study. *Acta Biomaterialia*, 8(4):1648–1658.

[Urban et al., 1977] Urban, J., Holms, S., Maroudas, A., and Nachemson, A. (1977). Nutrition of the intervertebral disc: An in vivo study of solute transport. *Clinical Orthopaedics and Related Research*, (129):101–114.

[Vidotto et al., 2019] Vidotto, M., Botnariuc, D., De Momi, E., and Dini, D. (2019). A computational fluid dynamics approach to determine white matter permeability. *Biomechanics and Modeling in Mechanobiology*, 18(4):1111–1122.

[Vidotto et al., 2018] Vidotto, M., Dini, D., and Momi, E. D. (2018). Effective Diffusion and Tortuosity in Brain White Matter. In *2018 40th Annual International Conference of the IEEE Engineering in Medicine and Biology Society (EMBC)*, volume 2018-July, pages 4901–4904. IEEE.

[Vigneswaran et al., 2015] Vigneswaran, K., Neill, S., and Hadjipanayis, C. G. (2015). Beyond the World Health Organization grading of infiltrating gliomas: Advances in the molecular genetics of glioma classification. *Annals of Translational Medicine*, 3(7):1–13.

[von Bartheld et al., 2016] von Bartheld, C. S., Bahney, J., and Herculano-Houzel, S. (2016). The search for true numbers of neurons and glial cells in the human brain: A review of 150 years of cell counting. *Journal of Comparative Neurology*, 524(18):3865–3895.

[Vunjak-Novakovic et al., 1999] Vunjak-Novakovic, G., Martin, I., Obradovic, B., Treppo, S., Grodzinsky, A. J., Langer, R., and Freed, L. E. (1999). Bioreactor cultivation conditions modulate the composition and mechanical properties of tissue-engineered cartilage. *Journal of Orthopaedic Research*, 17(1):130–138.

[Walhovd et al., 2014] Walhovd, K., Johansen-Berg, H., and Káradóttir, R. (2014). Unraveling the secrets of white matter – Bridging the gap between cellular, animal and human imaging studies. *Neuroscience*, 276:2–13.

[Wang et al., 2010] Wang, Y., Tomlins, P. E., Coombes, A. G., and Rides, M. (2010). On the Determination of Darcy Permeability Coefficients for a Microporous Tissue Scaffold. *Tissue Engineering Part C: Methods*, 16(2):281–289.

[Weiss and Maakestad, 2006] Weiss, J. A. and Maakestad, B. J. (2006). Permeability of human medial collateral ligament in compression transverse to the collagen fiber direction. *Journal of Biomechanics*, 39(2):276–283.

[Wells, 2008] Wells, R. G. (2008). The role of matrix stiffness in regulating cell behavior. *Hepatology*, 47(4):1394–1400.

[Wilson et al., 2014] Wilson, T., Karajannis, M., and Harter, D. (2014). Glioblastoma multiforme: State of the art and future therapeutics. *Surgical Neurology International*, 5(1):64.

[Winklewski et al., 2018] Winklewski, P. J., Sabisz, A., Naumczyk, P., Jodzio, K., Szurowska, E., and Szarmach, A. (2018). Understanding the Physiopathology Behind Axial and Radial Diffusivity Changes—What Do We Know? *Frontiers in Neurology*, 9(FEB).

[Yakar et al., 2018] Yakar, F., Eroglu, U., Peker, E., Armagan, E., Comert, A., and Ugur, H. C. (2018). Structure of corona radiata and tapetum fibers in ventricular surgery. *Journal of Clinical Neuroscience*, 57:143–148.

[Zhan et al., 2019] Zhan, W., Rodriguez y Baena, F., and Dini, D. (2019). Effect of tissue permeability and drug diffusion anisotropy on convection-enhanced delivery. *Drug Delivery*, 26(1):773–781.

[Zhang et al., 2000] Zhang, X.-Y., Luck, J., Dewhirst, M. W., and Yuan, F. (2000). Interstitial hydraulic conductivity in a fibrosarcoma. *American Journal of Physiology-Heart and Circulatory Physiology*, 279(6):H2726–H2734.

[Zhou et al., 2013] Zhou, J., Patel, T. R., Sirianni, R. W., Strohbehn, G., Zheng, M.-Q., Duong, N., Schafbauer, T., Huttner, A. J., Huang, Y., Carson, R. E., Zhang, Y., Sullivan, D. J., Piepmeier, J. M., and Saltzman, W. M. (2013). Highly penetrative, drug-loaded nanocarriers improve treatment of glioblastoma. *Proceedings of the National Academy of Sciences*, 110(29):11751–11756.